Postprint of: Chróścielewski J., Sabik A., Sobczyk B., Witkowski W., Nonlinear FEM 2D failure onset prediction of composite shells based on 6-parameter shell theory, Thin-Walled Structures, Vol. 105 (2016), pp. 207-219, DOI: 10.1016/j.tws.2016.03.024

Nonlinear FEM 2D Failure Onset Prediction of Composite Shells Based on 6-parameter Shell Theory

Chróścielewski J. [a] **(e-mail: jchrost@pg.gda.pl)**

Sabik A. [a] **(e-mail: agsa@pg.gda.pl),**

Sobczyk B. [a] **(e-mail: barsobcz@pg.gda.pl) - corresponding author**

Witkowski W [a] **(e-mail: wojwit@pg.gda.pl).**

[a] Gdańsk University of Technology, Faculty of Civil and Environmental Engineering, Department of Mechanics of Materials, 80-233 Gdańsk, Narutowicza 11/12, Poland

Highlights

- nonlinear 6 parameter shell theory, drilling rotation, asymmetric strain measures
- material law for shells with Cosserat type kinematics in FPF analysis
- Tsai-Wu and Hashin criteria modifications, satisfying the theory requirements
- FPF loads estimations for theories with symmetric and asymmetric strain measures
- quantitative and qualitative comparison of results

Nonlinear FEM 2D Failure Onset Prediction of Composite Shells Based on 6-parameter Shell Theory

Chróścielewski J. [a] **(e-mail: jchrost@pg.gda.pl)**

Sabik A. [a] **(e-mail: agsa@pg.gda.pl),**

Sobczyk B. [a] **(e-mail: barsobcz@pg.gda.pl) - corresponding author**

Witkowski W [a] **(e-mail: wojwit@pg.gda.pl).**

[a] Gdańsk University of Technology, Faculty of Civil and Environmental Engineering, Department of Mechanics of Materials, 80-233 Gdańsk, Narutowicza 11/12, Poland

Abstract

Within the framework of the nonlinear 6-parameter shell theory with the drilling rotation and asymmetric stress measures, the modifications of Tsai-Wu and Hashin laminate failure initiation criteria are proposed. These improvements enable to perform first ply failure estimations taking into account the non-symmetric stress measures. In order to check the validity of the proposed criteria, finite element analyses are performed with the use of the Authors' program and the Abaqus package. It is shown that the classical forms of the well known failure hypotheses can predict different stress capacity of structure, if the stress measures do not preserve the symmetry condition.

Keywords: first ply failure, finite element analysis, composite laminate, laminated shell, nonlinear six-parameter shell theory, drilling rotation

1. Introduction

This work is focused on the modelling of laminates, in particular on the appropriate estimation of failure initiation in structural laminated shells composed of intersecting panels. The problem is of great importance due to the increasing application of laminated shells in engineering solutions (see [1], [2]). Hence, a special attention is paid on estimation of their load capacity. Since laminated composites are anisotropic or orthotropic continua, the problem is quite complex and therefore refined failure criteria are required. It seems that up till now no universal hypothesis has been proposed. The existing failure theories base usually on the stress or strain state in each layer.

Composite laminates as thin structures in general, are usually modelled as shell-like bodies. From the point of view of the failure analysis, the adopted assumptions of shell kinematics should be efficient enough to describe structural behaviour together with the stress state in all layers. Most of the common shell theories relies on the symmetry of stress and strain measures. In this work, however, the proposed laminate model is based on the nonlinear 6-parmeter shell theory (6p theory). The sixth parameter is the rotation perpendicular to the shell reference surface. As such, the kinematical model of the 6p theory of shells is equivalent to that of Cosserat surface with three rigid directors and asymmetric stress and strain measures. Such an approach meets the requirements of the correct modelling of intersecting shells.

The foundation of the 6p shell theory may be traced back to the works of Reissner [3] and Libai and Simmonds [4]. Some of the recent advances may be found in e.g. [5], [6], [7], [8], [9], [10], [11], [12], [13]. The key characteristics of the 6p shell theory used in this paper are:

- 2D equilibrium equations of the shell-like body are obtained in the course of direct and exact through-the-thickness integration of 3D balance laws of linear and angular momentum of the Cauchy continuum,
- definitions of the shell strain measures follow directly from an integral identity resulting from the exact equilibrium equations, which make the theory kinematically unique,
- the strain and stress measures are not symmetric.

The 6p theory is formulated in such a way that all the simplifications appear on the level of the material law only.

The natural presence of the drilling rotation allows one for straightforward analysis of smooth as well as irregular shells both theoretically and with the aid of FEM. The irregular shells are composed of smooth shells connected along common edges that ultimately create a spatial shell structure. Their examples of application in engineering community are thin-walled members for instance. A thorough exposition to this field has recently been presented by Pietraszkiewicz and Konopińska [14].

Much work has been done on analyzes of elastic homogenous isotropic thin shells e.g. [15], [16], [17], [18], [19] [20] using the constitutive equations motivated in the early work of Makowski & Stumpf [21]. The equations are expressed in terms of Young's modulus and Poisson's ratio.

Altenbach and Eremeyev proposed in [22] the Cosserat plate theory with appropriate constitutive relations for elastic behaviour. The mutual relations between their approach and that of e.g. [15], [16], [17], [18], [19] were the topic of the paper [23] and its continuation [24].

The next approach to formulate the constitutive relation for the 6p shell theory is linked directly to the Cosserat continuum. Starting from plane stress of the Cosserat medium [25], and employing trough-the-thickness integration under the Reissner-Mindlin hypothesis (the

first-order shear deformation theory FSDT) in [26], [27], [28] the relations between stress and couple resultants and the shell strain measures were established for elastic and plastic behaviour. They depend not only Young's modulus and Poisson's ratio but rely also on the micropolar characteristic length l (material parameter) and the Cosserat coupling number [29], [30], [31]. Motivated by [26], [27], [28] Daszkiewicz et al. [32] have successfully derived the constitutive relations for shells made of functionally graded materials appropriate for the present 6p theory.

In this paper we follow the route proposed for composite shells in [33]. The suitable material law accounting for layered material structure in 6p shell theory has been derived from the asymmetric Cauchy-type plane stress relation. The through-the-thickness integration together with kinematical assumption of the first-order shear deformation theory provided the equivalent single-layer constitutive relation for composite shells in terms of five material engineering constants. Taking next step forward from there, we present here modifications of some failure criteria for laminates.

Commonly used stress-based failure initiation criteria for laminates, which are available in leading commercial FEM codes are: maximum stress, Tsai-Hill [35], Tsai-Wu [36], Hashin [37], Puck [38]. All these theories take into account the symmetry of stress measures. They are widely discussed and confronted with experimental results in [42]. Since the existing methods of initial failure determination do not account for the strain and stress measures asymmetry, their direct implementation into the unique shell theory used here is impossible. Therefore, we propose some modifications of the Tsai-Wu and Hashin criteria, that meet the requirements dictated by the nonlinear 6p shell theory. The particular constitutive relation is described in detail in chapter 4. In order to judge whether the criteria modifications are reasonable, some First Ply Failure (FPF) numerical analyses are carried out. Calculations are performed in the own Fortran code CAM [15], [16], and Abaqus. In the CAM code the non-

linear 6p shell theory is implemented together with modified failure initiation criteria, while the standard assumption of stress tensor symmetry and standard criteria versions are used in Abaqus. The numerical examples are presented to show the performance of the proposed approach with the attention focused on irregular shells.

2. Weak formulation of the boundary value problem

The purpose of this section is to provide the necessary background lying behind the used finite element code CAM. We provide only summary of the most important aspects of the formulation. The equations of motion, strong and weak formulation for the present 6p shell theory have been discussed in detail in previous works e.g. [15], [16], [17], [18] and in the references given there.

Within the general theory of irregular shell structures, the initial (undeformed) configuration of the 3D shell-like body is represented by a 2D surface-like continuum M called briefly an (undeformed) reference network, [39], [40], see Figure 1.

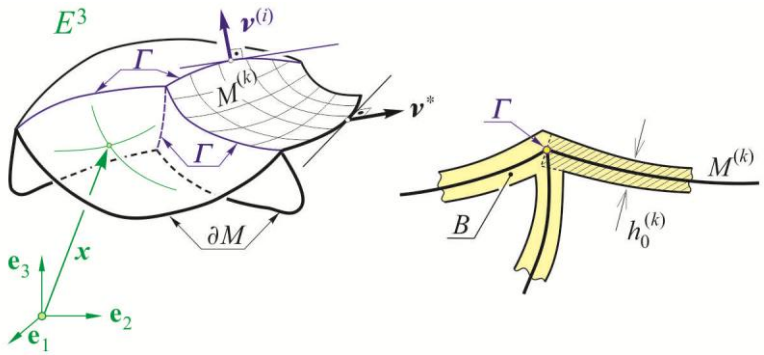

Figure 1. General irregular shell structures

The network $M = \bigcup_{k=1,2,..,K} M^{(k)}$ consists of a finite number of regular surface elements $M^{(k)}$, $k = 1, 2, ..., K$, joined together along parts of their boundaries $\partial M^{(k)}$. Each $M^{(k)}$ is a bounded, oriented, connected and smooth surface whose boundaries $\partial M^{(k)}$ consist of a finite number of closed, piecewise smooth curves. Common parts of boundaries of all surfaces $M^{(k)}$ form a

spatial curve $\Gamma = \bigcup_{\substack{k,m=1,2,..,K \\ k \neq m}} \partial M^{(k)} \cap \partial M^{(m)}$ (Fig. 1) called a singular curve $\Gamma \subset M$. Therefore, the boundary base surface of general irregular shell structures is $\partial M = \left(\bigcup_{k=1,2,..,K} \partial M^{(k)} \right) \setminus \Gamma$.

We further assume that the boundary ∂M is a union $\partial M = \partial M_d \cup \partial M_f$, $\partial M_d \cap \partial M_f = \varnothing$ where displacement (d) and traction (f) boundary conditions are imposed, respectively. It is assumed that $M \setminus \Gamma$ is smooth enough for the existence of the metric and the curvature tensors. Each typical regular point $\boldsymbol{x} \in M \setminus \Gamma$ is described by the pair $(\boldsymbol{x}, \boldsymbol{T}_0)$, where $\boldsymbol{x} \in E^3$ (E^3 being the Euclidean space) is the position vector and $\boldsymbol{T}_0 \in SO(3)$ is the structure tensor composed of directors

$$\boldsymbol{t}_\beta^0 = \boldsymbol{x}_{,\beta}, \quad \boldsymbol{t}^0 \equiv \boldsymbol{t}_3^0 = \frac{\boldsymbol{t}_1^0 \times \boldsymbol{t}_2^0}{\| \boldsymbol{t}_1^0 \times \boldsymbol{t}_2^0 \|}, \quad \beta = 1,2, \quad (.)_{,\beta} = \frac{\partial (.)}{\partial s^\beta} \tag{1}$$

with $SO(3)$ as the special orthogonal group. In FEM approach we assume that the vector $\boldsymbol{x}$ and the triad $\{\boldsymbol{t}_i^0\}$ are the given data of the analyzed shell. Here we take the directors $\{\boldsymbol{t}_i^0\}$ as the rigid orthogonal frame i.e. $\boldsymbol{t}_i^0 \cdot \boldsymbol{t}_j^0 = \delta_{ij}$, $\boldsymbol{t}_i^0 = \boldsymbol{t}_0^i$, $\boldsymbol{t}^0 \equiv \boldsymbol{t}_0^3$, $\| \boldsymbol{t}_i^0 \| = 1$.

The deformation of such reference network M is uniquely described by two fields: the position vector field $\boldsymbol{y}(\boldsymbol{x}) = \boldsymbol{u}(\boldsymbol{x}) + \boldsymbol{x}$ that represents the translatory deformation of the shell reference network, and the proper orthogonal tensor field $\boldsymbol{T}(\boldsymbol{x}) = \boldsymbol{T}_0(\boldsymbol{x}) \boldsymbol{Q}(\boldsymbol{x})$, where $\boldsymbol{Q}(\boldsymbol{x})$ represents the mean rotary deformation of the shell cross sections. Here we restrict ourselves only to geometric irregularities and allow the shell to have only folds, branches and/or self-intersections. We assume from the beginning that the kinematic fields $\boldsymbol{y}(\boldsymbol{x})$ and $\boldsymbol{Q}(\boldsymbol{x})$ are continuous during the motion, and $\boldsymbol{y}_\Gamma(\boldsymbol{x}_\Gamma) = \boldsymbol{y}(\boldsymbol{x})|_\Gamma$, $\boldsymbol{u}_\Gamma(\boldsymbol{x}_\Gamma) = \boldsymbol{u}(\boldsymbol{x})|_\Gamma$, $\boldsymbol{Q}_\Gamma(\boldsymbol{x}_\Gamma) = \boldsymbol{Q}(\boldsymbol{x})|_\Gamma$, with

$\boldsymbol{x}_\Gamma \in \Gamma$. Hence, we do not associate any mechanical properties with the singular curve Γ itself.

Configuration space of the shell is defined as

$$U = C(M,G) = \left\{ \mathbf{u} = (\boldsymbol{u},\boldsymbol{Q}) : M \to G = E^3 \times SO(3) \right\}. \tag{2}$$

$\boldsymbol{Q}(\boldsymbol{x}) \in SO(3)$ is an independent proper orthogonal tensor. The space tangent to (2) at $\mathbf{u}$ is

$$W = T_{\mathbf{u}}U \approx C(M,G) = \left\{ \mathbf{w} = (\boldsymbol{v},\boldsymbol{w}) : M \to G = E^3 \times so(3) \right\}, \tag{3}$$

where we define the continuous virtual vector fields of translations $\boldsymbol{v}(\boldsymbol{x}) \in E^3$ and rotations $\boldsymbol{w}(\boldsymbol{x}) \in so(3)$ with $so(3)$ being the space of skew-symmetric tensors. Due to the isomorphism $so(3) \approx E^3$ it is also true that

$$T_{\mathbf{u}}U \approx C(M,E) = \left\{ \mathbf{w} = (\boldsymbol{v},\boldsymbol{w}) : M \to E = E^3 \times E^3 \right\} \quad . \tag{4}$$

After deformation $\mathbf{u} = (\boldsymbol{u},\boldsymbol{Q})$ the current position $\boldsymbol{y}(\boldsymbol{x})$ and the current microstructure tensor $\boldsymbol{T}(\boldsymbol{x}) \in SO(3)$ are given by the vector fields: $\boldsymbol{y}(\boldsymbol{x}) = \boldsymbol{u}(\boldsymbol{x}) + \boldsymbol{x}$ and $\boldsymbol{t}_i(\boldsymbol{x}) = \boldsymbol{Q}(\boldsymbol{x})\boldsymbol{t}_i^0(\boldsymbol{x}) = \boldsymbol{Q}(\boldsymbol{x})\boldsymbol{T}_0(\boldsymbol{x})\mathbf{e}_i = \boldsymbol{T}(\boldsymbol{x})\mathbf{e}_i$.

To formulate the weak form of the problem we define the following spaces: the space of kinematically admissible displacement fields satisfying the prescribed boundary conditions $\mathbf{u}^* = (\boldsymbol{u}^*,\boldsymbol{Q}^*)$ on ∂M_d,

$$U \equiv C(M,G) = \left\{ \mathbf{u} : \mathbf{u}(\boldsymbol{x}) = \mathbf{u}^*(\boldsymbol{x});\ \boldsymbol{x} \in \partial M_d \right\}, \tag{5}$$

and the space of kinematically admissible displacement fields satisfying the homogenous boundary conditions $\mathbf{w}(\boldsymbol{x}) = \mathbf{0}$ on ∂M_d,

$$V \equiv C(M, E^3 \times E^3) = \left\{ \mathbf{w} : w_i \in H^1;\ \mathbf{w}(\boldsymbol{x}) = \mathbf{0};\ \boldsymbol{x} \in \partial M_d \right\}, \tag{6}$$

where $H^1 = \{w : w \in L_2;\ w_{,x} \in L_2\}$ is the Hilbert space of square-integrable functions such that $L_2(B) = \left\{w : \int_B w^2 dx < \infty\right\}$.

The definition of shell strain measures in the defined basis is given by ([15], [16], [17], [18], [21]):

$$\tilde{\boldsymbol{\varepsilon}}(\mathbf{u}) = \begin{Bmatrix} \boldsymbol{\varepsilon}_\beta \\ \boldsymbol{\kappa}_\beta \end{Bmatrix} = \begin{Bmatrix} \boldsymbol{\varepsilon}_1 \\ \boldsymbol{\varepsilon}_2 \\ \boldsymbol{\kappa}_1 \\ \boldsymbol{\kappa}_2 \end{Bmatrix} = \begin{Bmatrix} \boldsymbol{u}_{,1} + (\mathbf{1} - \boldsymbol{Q})\boldsymbol{t}_1^0 \\ \boldsymbol{u}_{,2} + (\mathbf{1} - \boldsymbol{Q})\boldsymbol{t}_2^0 \\ \operatorname{axl}(\boldsymbol{Q}_{,1}\boldsymbol{Q}^{\mathrm{T}}) \\ \operatorname{axl}(\boldsymbol{Q}_{,2}\boldsymbol{Q}^{\mathrm{T}}) \end{Bmatrix}, \quad \delta\tilde{\boldsymbol{\varepsilon}} = \begin{Bmatrix} \delta\boldsymbol{\varepsilon}_1 \\ \delta\boldsymbol{\varepsilon}_2 \\ \delta\boldsymbol{\kappa}_1 \\ \delta\boldsymbol{\kappa}_2 \end{Bmatrix} = \begin{Bmatrix} \boldsymbol{v}_{,1} + (\boldsymbol{t}_1 + \boldsymbol{\varepsilon}_1) \times \boldsymbol{w} \\ \boldsymbol{v}_{,2} + (\boldsymbol{t}_2 + \boldsymbol{\varepsilon}_2) \times \boldsymbol{w} \\ \boldsymbol{w}_{,1} \\ \boldsymbol{w}_{,2} \end{Bmatrix}, \tag{7}$$

where the axial vector of the skew tensor is defined with operator $\operatorname{axl}(...)$. For convenience the above equations are put into compact notation

$$\tilde{\boldsymbol{\varepsilon}}(\mathbf{u}) = \mathbf{B}(\mathbf{u})\mathbf{u}, \quad \delta\tilde{\boldsymbol{\varepsilon}}(\mathbf{u}) = \mathbf{B}(\mathbf{u})\mathbf{w}, \quad \mathbf{B}(\mathbf{u}) = \begin{bmatrix} \mathbf{1}(.)_{,1} & (\boldsymbol{t}_1 + \boldsymbol{\varepsilon}_1) \times (.) \\ \mathbf{1}(.)_{,2} & (\boldsymbol{t}_2 + \boldsymbol{\varepsilon}_2) \times (.) \\ \mathbf{0} & \mathbf{1}(.)_{,1} \\ \mathbf{0} & \mathbf{1}(.)_{,2} \end{bmatrix}. \tag{8}$$

The external resultant load vector $\mathbf{p}(\boldsymbol{x})$ and the vector of the prescribed boundary loads $\mathbf{s}^*$, $\mathbf{s}_\Gamma$ read

$$\mathbf{p}(\boldsymbol{x}) = \begin{Bmatrix} \boldsymbol{f}(\boldsymbol{x}) \\ \boldsymbol{c}(\boldsymbol{x}) \end{Bmatrix} \text{ on } M \setminus \Gamma, \qquad \mathbf{s}^* = \begin{Bmatrix} \boldsymbol{n}^* \\ \boldsymbol{m}^* \end{Bmatrix} \text{ on } \partial M_f, \qquad \mathbf{s}_\Gamma = \begin{Bmatrix} \boldsymbol{n}_\Gamma \\ \boldsymbol{m}_\Gamma \end{Bmatrix} \text{ on } \Gamma, \tag{9}$$

where $\boldsymbol{f}(\boldsymbol{x})$ is the external resultant force vector field and $\boldsymbol{c}(\boldsymbol{x})$ is the external resultant couple vector field on $M \setminus \Gamma$. The components $\boldsymbol{n}^*(\boldsymbol{x})$ and $\boldsymbol{m}^*(\boldsymbol{x})$ are the prescribed boundary tractions and couples along ∂M_f, while components $\boldsymbol{n}_\Gamma(\boldsymbol{x})$ and $\boldsymbol{m}_\Gamma(\boldsymbol{x})$ are their counterparts defined along the singular curve $\Gamma \subset M$.

The constitutive relation is assumed in the general form

$$\mathbf{S} = \tilde{\mathbf{S}}\left(\tilde{\boldsymbol{\varepsilon}}(\mathbf{u})\right) = \tilde{\mathbf{S}}(\mathbf{u}) \quad \text{on} \quad M \setminus \Gamma. \tag{10}$$

In the introduced notation the external virtual work is defined as

$$\langle\langle \mathbf{p}, \mathbf{w} \rangle\rangle_{M\setminus\Gamma} + \langle \mathbf{s}^*, \mathbf{w} \rangle_{\partial M_f} + \langle \mathbf{s}_\Gamma, \mathbf{w} \rangle_\Gamma = \iint_{M\setminus\Gamma} (\boldsymbol{f}\cdot\boldsymbol{v} + \boldsymbol{c}\cdot\boldsymbol{w})\, da + \int_{\partial M_f} (\boldsymbol{n}^*\cdot\boldsymbol{v} + \boldsymbol{m}^*\cdot\boldsymbol{w}) ds + \int_\Gamma (\boldsymbol{n}_\Gamma\cdot\boldsymbol{v} + \boldsymbol{m}_\Gamma\cdot\boldsymbol{w}) ds. \tag{11}$$

The internal virtual work reads

$$\langle\langle \tilde{\mathbf{S}}(\mathbf{u}), \mathbf{B}(\mathbf{u})\mathbf{w} \rangle\rangle_{M\setminus\Gamma} = \iint_{M\setminus\Gamma} [\boldsymbol{n}^\beta\cdot(\boldsymbol{v}_{,\beta} + \boldsymbol{y}_{,\beta}\times\boldsymbol{w}) + \boldsymbol{m}^\beta\cdot\boldsymbol{w}_{,\beta}]\, da\,. \tag{12}$$

The internal stress and couple resultant vectors $\boldsymbol{n}^\beta(\boldsymbol{x})$ and $\boldsymbol{m}^\beta(\boldsymbol{x})$, respectively, are primary variables of the theory. Here, to define them we use the constitutive relation (10).

In the spaces defined above the principle of virtual work is stated as follows: given the external resultant force and couple vector fields $\boldsymbol{f}(\boldsymbol{x})$ and $\boldsymbol{c}(\boldsymbol{x})$ on $\boldsymbol{x}\in M\setminus\Gamma$, $\boldsymbol{n}^*(\boldsymbol{x})$ and $\boldsymbol{m}^*(\boldsymbol{x})$ along ∂M_f, $\boldsymbol{n}_\Gamma(\boldsymbol{x})$ and $\boldsymbol{m}_\Gamma(\boldsymbol{x})$ along the singular curve $\Gamma\subset M$, find a curve $\mathbf{u}(\boldsymbol{x}) = (\boldsymbol{u}(\boldsymbol{x}), \boldsymbol{Q}(\boldsymbol{x}))$ on the configuration space (2) such that for any continuous, kinematically admissible virtual vector fields the following identity is satisfied

$$\langle\langle \tilde{\mathbf{S}}(\mathbf{u}), \mathbf{B}(\mathbf{u})\mathbf{w} \rangle\rangle_M = \langle\langle \mathbf{p}, \mathbf{w} \rangle\rangle_M + \langle \mathbf{s}^*, \mathbf{w} \rangle_{\partial M_f} + \langle \mathbf{s}_\Gamma, \mathbf{w} \rangle_\Gamma \tag{13}$$

with the kinematic boundary conditions $\boldsymbol{u}(\boldsymbol{x}) = \boldsymbol{u}^*(\boldsymbol{x})$ and $\boldsymbol{Q}(\boldsymbol{x}) = \boldsymbol{Q}^*(\boldsymbol{x})$ satisfied on the complementary part $\partial M_d = \partial M\setminus\partial M_f$. We take the virtual vector fields as kinematically admissible if $\boldsymbol{v}(\boldsymbol{x}) = \mathbf{0}$ and $\boldsymbol{w}(\boldsymbol{x}) = \mathbf{0}$ on ∂M_d.

3. Finite element approximation

Relation (13) undergoes linearization [15], providing the base for spatial approximation, see Figure 2

$$M \approx M_h = \sum_{e=1}^{N_e} \Pi_{(e)}\,. \tag{14}$$

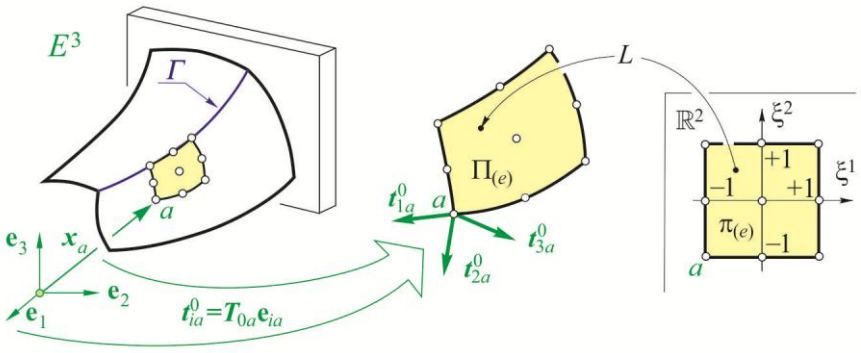

Figure 2. Global frame, typical element and natural element

Here $\Pi_{(e)}$ is a typical finite element defined as a smooth image of the standard element $\pi_{(e)}=[-1,+1]\times[-1,+1]$ from the parent (natural) domain $\boldsymbol{\xi}=(\xi_1,\xi_2)$. On the element level the vector field variables undergo standard interpolation using generic formula $[...](\boldsymbol{\xi})=\sum_{i=1}^{N_w}L_i(\boldsymbol{\xi})[...]_i$ with $L_i(\boldsymbol{\xi})$ as the Lagrange polynomials being the members of the space of interpolating functions

$$\Lambda_{(e)}=\left\{ L_i(\boldsymbol{\xi}):L_i(\boldsymbol{\xi}_j)=\delta_{ij},\ \sum_{i=1}^{N_w}L_i(\boldsymbol{\xi})=1,\ \forall\boldsymbol{\xi}\in\pi_{(e)} \right\}. \tag{15}$$

The resulting elements are C^0 class. In passing, reference [34] contains interesting approach to geometrically exact shell theory based on Kirchhoff-Love kinematics. In the present approach all the variables from $SO(3)$ group undergo C^0 interpolation that relies on the approach described in [17], [18], [33]. Briefly, the approach is based on some kind of transport of the interpolation domain to the neighbourhood of the neutral element of the $SO(3)$ group. Thereby, it becomes singularity-free. The proposed approach is independent of selected parameterization cf. for instance [43], [44], [45]. Here we employ the canonical parameterization. Throughout the text, the finite elements described here, are denoted as CAM*e*n [15], where the natural number n denotes the total number of nodes i.e. 4 (2×2), 9 (3×3) or 16 (4×4). The elements are integrated by Gauss-Legendre rule with either full integration (FI) or uniform reduced integration (URI).

4. Constitutive relation, failure criteria

As a special form of the constitutive relation (10) we assume

$$\mathbf{s} = \mathbf{C}\boldsymbol{\varepsilon}, \text{ on } M \setminus \Gamma, \tag{16}$$

where the shell strain measures (7) and corresponding stress and couple resultants are given in the spatial representation ($\{\boldsymbol{t}_i(\boldsymbol{x}), i=1,2,3\}$)

$$\boldsymbol{\varepsilon} = \{\varepsilon_{11}\ \varepsilon_{22}\ \varepsilon_{12}\ \varepsilon_{21}|\varepsilon_1\ \varepsilon_2\|\kappa_{11}\ \kappa_{22}\ \kappa_{12}\ \kappa_{21}|\kappa_1\ \kappa_2\}^T = \{\boldsymbol{\varepsilon}_m|\boldsymbol{\varepsilon}_s\|\boldsymbol{\varepsilon}_b|\boldsymbol{\varepsilon}_d\}^T, \tag{17}$$

$$\mathbf{s} = \{N^{11}N^{22}N^{12}N^{21}|Q^1Q^2\|M^{11}M^{22}M^{12}M^{21}|M^1M^2\}^T = \{\mathbf{s}_m|\mathbf{s}_s\|\mathbf{s}_b|\mathbf{s}_d\}^T. \tag{18}$$

Since FPF analysis is taken into account in this paper, we assume that $\mathbf{C}$ remains, by assumption, constant during the analysis, though it may vary between the elements. As discussed in [33] for the present 6p theory $\mathbf{C}$ may be obtained by assuming plane stress in each lamina k in the material axes

$$\begin{Bmatrix} \sigma_{aa} \\ \sigma_{bb} \\ \sigma_{ab} \\ \sigma_{ba} \\ \hline \sigma_a \\ \sigma_b \end{Bmatrix}_k = \left[\begin{array}{cccc|cc} \frac{E_a}{1-\nu_{ab}\nu_{ba}} & \frac{\nu_{ab}E_b}{1-\nu_{ab}\nu_{ba}} & 0 & 0 & 0 & 0 \\ \frac{\nu_{ba}E_a}{1-\nu_{ab}\nu_{ba}} & \frac{E_b}{1-\nu_{ab}\nu_{ba}} & 0 & 0 & 0 & 0 \\ 0 & 0 & 2G_{ab} & 0 & 0 & 0 \\ 0 & 0 & 0 & 2G_{ab} & 0 & 0 \\ \hline 0 & 0 & 0 & 0 & 2G_{ac} & 0 \\ 0 & 0 & 0 & 0 & 0 & 2G_{bc} \end{array}\right]_k \begin{Bmatrix} \varepsilon^{aa} \\ \varepsilon^{bb} \\ \varepsilon^{ab} \\ \varepsilon^{ba} \\ \hline \varepsilon^{a} \\ \varepsilon^{b} \end{Bmatrix}_k, \tag{19}$$

$$\begin{Bmatrix} \boldsymbol{\sigma}_m^{mat} \\ \hline \boldsymbol{\sigma}_s^{mat} \end{Bmatrix}_k = \left[\begin{array}{c|c} \tilde{\boldsymbol{C}}_m & \mathbf{0}_{4\times 2} \\ \hline \mathbf{0}_{4\times 2} & \tilde{\boldsymbol{C}}_s \end{array}\right]_k \begin{Bmatrix} \boldsymbol{\varepsilon}_m^{mat} \\ \hline \boldsymbol{\varepsilon}_s^{mat} \end{Bmatrix}_k = \tilde{\boldsymbol{C}}_k \begin{Bmatrix} \boldsymbol{\varepsilon}_m^{mat} \\ \hline \boldsymbol{\varepsilon}_s^{mat} \end{Bmatrix}_k. \tag{20}$$

In (19) the following definitions hold: $(E_a)_k$, $(E_b)_k$ are the Young moduli in material axes, $(G_{ab})_k$ is the in-plane shear modulus in material axes, $(\nu_{ab})_k$, $(\nu_{ba})_k$ are the Poisson ratios that satisfy the condition $E_a\nu_{ba} = E_b\nu_{ab}$ (no summation), and $(G_{ac})_k, (G_{bc})_k$ are the transverse shear moduli.

Relation (19), which undergoes transformation to the $\{\boldsymbol{t}_i^0\}$ base and through-the-thickness integration of appropriate terms from (19) under FSDT assumption, yields the equivalent single-layer constitutive relations [33]

$$\mathbf{s}_m = \sum_{k=1}^{N_L}\left(\int_{\zeta_k^-}^{\zeta_k^+}\{\boldsymbol{C}_m\}_k\left(\boldsymbol{\varepsilon}_m+\zeta\boldsymbol{\varepsilon}_b\right)\mu\,d\zeta\right)=\underset{4\times4}{\mathbf{A}}\,\boldsymbol{\varepsilon}_m+\underset{4\times4}{\mathbf{B}}\,\boldsymbol{\varepsilon}_b, \tag{21}$$

$$\mathbf{s}_s = \sum_{k=1}^{N_L}\left(\int_{\zeta_k^-}^{\zeta_k^+}(\alpha_s)_k\{\boldsymbol{C}_s\}_k\boldsymbol{\varepsilon}_s\,\mu\,d\zeta\right)=\underset{2\times2}{\mathbf{S}}\,\boldsymbol{\varepsilon}_s, \tag{22}$$

$$\mathbf{s}_b = \sum_{k=1}^{N_L}\left(\int_{\zeta_k^-}^{\zeta_k^+}\{\boldsymbol{C}_m\}_k\left(\zeta\boldsymbol{\varepsilon}_m+(\zeta)^2\boldsymbol{\varepsilon}_b\right)\mu\,d\zeta\right)=\underset{4\times4}{\mathbf{B}}\,\boldsymbol{\varepsilon}_m+\underset{4\times4}{\mathbf{D}}\,\boldsymbol{\varepsilon}_b, \tag{23}$$

$$\mathbf{s}_d = \alpha_t\sum_{k=1}^{N_L}\left(\int_{\zeta_k^-}^{\zeta_k^+}(\alpha_t)_k\{\boldsymbol{C}_d\}_k\boldsymbol{\varepsilon}_d\,\mu\,d\zeta\right)=\underset{2\times2}{\mathbf{G}}\,\boldsymbol{\varepsilon}_d\ . \tag{24}$$

Here ζ_k^+ and ζ_k^- denote, respectively, the distance from the reference surface to the top and bottom of the k^{th} layer, μ is the determinant of the shifter tensor, $(\alpha_s)_k$ and $(\alpha_t)_k$ are the shear correction factors [19]. The remaining terms in (21)-(24) are specified in Appendix. Ultimately, correspondingly to (16) we have the following equation in matrix notation

$$\underset{12\times1}{\begin{Bmatrix}\mathbf{s}_m\\ \mathbf{s}_s\\ \mathbf{s}_b\\ \mathbf{s}_d\end{Bmatrix}}=\underset{12\times12}{\begin{bmatrix}\underset{4\times4}{\mathbf{A}} & \mathbf{0} & \underset{4\times4}{\mathbf{B}} & \mathbf{0}\\ \mathbf{0} & \underset{2\times2}{\mathbf{S}} & \mathbf{0} & \mathbf{0}\\ \underset{4\times4}{\mathbf{B}} & \mathbf{0} & \underset{4\times4}{\mathbf{D}} & \mathbf{0}\\ \mathbf{0} & \mathbf{0} & \mathbf{0} & \underset{2\times2}{\mathbf{G}}\end{bmatrix}}\underset{12\times1}{\begin{Bmatrix}\boldsymbol{\varepsilon}_m\\ \boldsymbol{\varepsilon}_s\\ \boldsymbol{\varepsilon}_b\\ \boldsymbol{\varepsilon}_d\end{Bmatrix}}. \tag{25}$$

The stress tensor under the constitutive relation (19) is not symmetric, therefore it is not possible to associate its components directly with existing failure initiation criteria. The Tsai-Wu criterion is a general polynomial criterion, applicable to arbitrary lamina types (e.g. unidirectional, biaxial). It was developed, assuming that a failure surface $f(\sigma_k)=F_i\sigma_i+F_{ij}\sigma_i\sigma_j=1\ \ i,j,k=1,2,...,6$ (written in contracted notation, see [36]) exists.

Thus, all stress tensor components that are available for the considered continuum (e.g. 3D or 2D plane stress) describe the failure surface in one expression [36].

The plane of failure is not identified according to the classical form of the criterion, hence a particular in-plane shear component cannot be clearly associated with the failure surface. Therefore, within the non-linear 6p shell theory used here the maximum value of the in-plane shear components ($\sigma_{ab} \neq \sigma_{ba}$) is introduced into the failure surface equation (see also [46], [47]). Thus, the most unfavourable situation in an engineering sense is considered regarding the stress state for FPF estimations. The proposed modification does not violate the generality of the classical criterion. The modified Tsai-Wu criterion takes the following form for the plane state of stress:

$$F_{TW} = \left(\frac{1}{X_t} - \frac{1}{X_c}\right)\sigma_{aa} + \left(\frac{1}{Y_t} - \frac{1}{Y_c}\right)\sigma_{bb} + \frac{1}{X_t X_c}\sigma_{aa}^2 + \frac{1}{Y_t Y_c}\sigma_{bb}^2 - \frac{1}{\sqrt{X_t X_c Y_t Y_c}}\sigma_{aa}\sigma_{bb} + \frac{\left[\max\left(|\sigma_{ab}|;|\sigma_{ba}|\right)\right]^2}{S_l^2}, \tag{26}$$

where X_t, Y_t denote the absolute values of tensile strength in the 1st and 2nd material axes, X_c, Y_c correspond to the absolute values of compressive strength in the 1st and 2nd material direction, whereas S_l is the shear strength in the layer plane. The failure occurs when the stress state yields $F_{TW} = 1$. In order to clearly present the differences between the standard and modified version of Tsai-Wu criterion we compare them in Table 1. Additionally, we introduce a specific notation, that clearly distinguishes symmetric τ_{ab} and asymmetric σ_{ab}, σ_{ba} in-plane shear stress components.

Table 1. Comparison of terms defining the failure surface in classical and modified Tsai-Wu criterion

The considered term	Standard criterion	Modified criterion
Linear normal term in *a* direction	$\left(\frac{1}{X_t}-\frac{1}{X_c}\right)\sigma_{aa}$	
Linear normal term in *b* direction	$\left(\frac{1}{Y_t}-\frac{1}{Y_c}\right)\sigma_{bb}$	
quadratic normal term in *a* direction	$\frac{1}{X_t X_c}\sigma_{aa}^2$	
quadratic normal term in *b* direction	$\frac{1}{Y_t Y_c}\sigma_{bb}^2$	
Interactive term	$-\frac{1}{\sqrt{X_t X_c Y_t Y_c}}\sigma_{aa}\sigma_{bb}$	
In-plane shear effects	$\frac{\tau_{ab}^2}{S_l^2}$	$\frac{\left[\max\left(\lvert\sigma_{ab}\rvert;\lvert\sigma_{ba}\rvert\right)\right]^2}{S_l^2}$

The Hashin criterion, as opposed to the Tsai-Wu theory, is able to predict the mode of damage. It is developed on the basis of four expressions, which correspond to: fibre tension (F_f^t), fibre compression (F_f^c), matrix tension (F_m^t) and matrix compression (F_m^c). It is not as general as the Tsai-Wu criterion, since it is applicable only to unidirectional laminas [37]. According to the original work of Hashin [37], the criterion is developed assuming that the failure is caused by normal and shear stress components, which act on a specific failure plane. Moreover, the failure surface is approximated with quadratic shape in the stress space relative to material coordinate system. For unidirectional material it can be stated that fibre failure occurs in the plane with its normal parallel to the 1st material axis.

The definition of failure plane for matrix failure is more complicated, since it is parallel to the fibres but may be inclined. Hashin [37] did not manage to describe the angle of matrix failure plane inclination. Therefore, he tried to express the failure process by means of all available stress tensor components, combined in quadratic expressions, excluding the normal

component in fibre direction. Hence, in order to modify Hashin criterion to 6p theory a correct interpretation of the action of in-plane shear ($\sigma_{ab} \neq \sigma_{ba}$) should be proposed, see also [46]. Consequently, σ_{ab} in-plane shear stress component is used in the fibre failure expression, as this component acts on the fibre failure plane. Modifying the matrix failure expressions, which in this case are limited only to in-plane influences, we may use: σ_{bb} , σ_{ab} , σ_{ba} , components (σ_{aa} is excluded). However, we also exclude σ_{ab} component, because its action does not induce cracks leading to matrix failure (parallel to fibres). In effect, we associate σ_{ba} with all terms connected with in-plane shear action. Thus, the modified Hashin criterion, proposed here for 6p theory, reads:

$$F_f^t = \left(\frac{\sigma_{aa}}{X_t}\right)^2 + \left(\frac{\sigma_{ab}}{S_l}\right)^2 \quad \text{for} \quad \sigma_a > 0\,, \tag{27}$$

$$F_f^c = \left(\frac{\sigma_{aa}}{X_c}\right)^2 \quad \text{for} \quad \sigma_a < 0\,, \tag{28}$$

$$F_m^t = \left(\frac{\sigma_{bb}}{Y_t}\right)^2 + \left(\frac{\sigma_{ba}}{S_l}\right)^2 \quad \text{for} \quad \sigma_b > 0\,, \tag{29}$$

$$F_m^c = \left(\frac{\sigma_{bb}}{2S_t}\right)^2 + \left[\left(\frac{Y_c}{2S_t}\right)^2 - 1\right]\frac{\sigma_{bb}}{Y_c} + \left(\frac{\sigma_{ba}}{S_l}\right)^2 \quad \text{for} \quad \sigma_b < 0\,, \tag{30}$$

where S_t denotes the transverse shear strength. It is understood that if one of the failure indices becomes equal to 1 the failure occurs. In order to portray the differences between the standard and modified version of Hashin criterion we collect them in Table 2.

Table 2. Comparison of terms defining the failure surface in standard and modified Hashin criterion

Mode of failure	Standard criterion	Modified criterion
(F_f^t)	$\left(\frac{\sigma_{aa}}{X_t}\right)^2+\left(\frac{\tau_{ab}}{S_l}\right)^2$	$\left(\frac{\sigma_{aa}}{X_t}\right)^2+\left(\frac{\sigma_{ab}}{S_l}\right)^2$
(F_f^c)	$\left(\frac{\sigma_{aa}}{X_c}\right)^2$	
(F_m^t)	$\left(\frac{\sigma_{bb}}{Y_t}\right)^2+\left(\frac{\tau_{ab}}{S_l}\right)^2$	$\left(\frac{\sigma_{bb}}{Y_t}\right)^2+\left(\frac{\sigma_{ba}}{S_l}\right)^2$
(F_m^c)	$\left(\frac{\sigma_{bb}}{2S_t}\right)^2+\left[\left(\frac{Y_c}{2S_t}\right)^2-1\right]\frac{\sigma_{bb}}{Y_c}+\left(\frac{\tau_{ab}}{S_l}\right)^2$	$\left(\frac{\sigma_{bb}}{2S_t}\right)^2+\left[\left(\frac{Y_c}{2S_t}\right)^2-1\right]\frac{\sigma_{bb}}{Y_c}+\left(\frac{\sigma_{ba}}{S_l}\right)^2$

5. Examples

5.1. Pure shear

Firstly, a 2D one-layer, square membrane, under plane-stress condition in pure shear is analysed. The aim of this task is to see how the standard and modified failure criteria (see Tab. 1 and Tab. 2) and the underlying theories respond to the state of pure shear. The dimensions, surface coordinate system (t_1-t_2), loads and boundary conditions (BCs) of the membrane are shown in Figure 3.

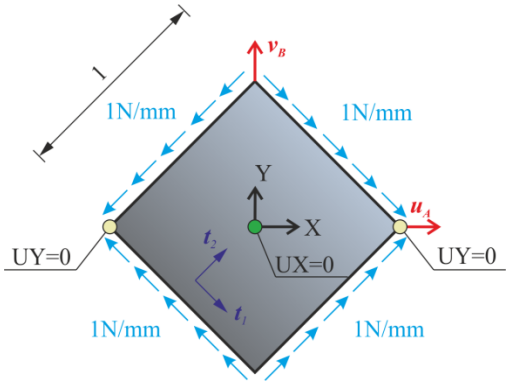

Figure 3. Geometry, surface coordinate system, loads and BCs of the membrane

A linear static analysis is carried out. The properties of the material are: $E_a = 45.0$ GPa, $E_b = 12.5$ GPa, $G_{ab} = G_{ac} = 5.5$ GPa, $G_{bc} = 3.6$ GPa, $v_{ab} = 0.28$. The membrane is 0.01mm

thick and has [0] orientation, relative to the surface coordinate system (see Figure 3). The mesh is built with different types of finite elements. The basic division is adjusted to CAMe4FI finite elements with 12 elements created on each edge. This particular division allows application of higher order finite elements, viz. CAMe9FI and CAMe16FI without the change of the total number and location of nodes in the mesh. Following regular meshes are analysed: 12×12 mesh of CAMe4FI and S4 (Abaqus), 6×6 mesh of CAMe9FI and finally 4×4 mesh of CAMe16FI elements. FI symbol indicates that the full integration procedure is associated with the finite element.

During the FEM calculations pure shear was recovered in all cases and the locking effect was not observed. The displacements u_A and v_b are the same for all computational variants, including Abaqus and CAM, as follows: $u_A = 6.428 \cdot 10^{-3}\text{mm}$, $v_B = -6.428 \cdot 10^{-3}\text{mm}$. The contours of displacement magnitudes obtained in calculations carried out by means of S4 (Abaqus) and CAMe4FI elements are presented in Figure 4.

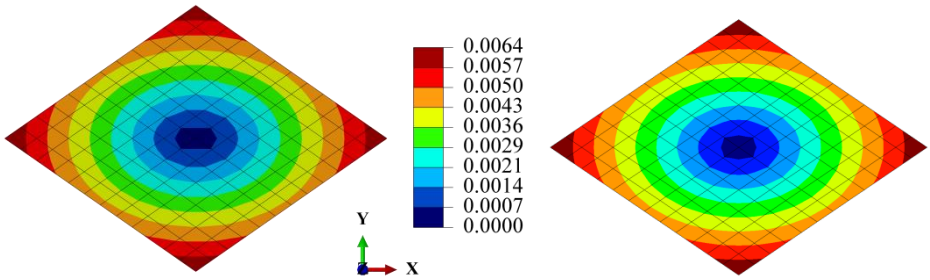

Figure 4. Contours of displacement magnitudes (scaled ×20): S4 (Abaqus, left) and CAMe4FI (right)

The normal stress tensor components are zeros in both codes in all elements. The drilling couples, included in 6p theory in CAM are zeros too. The in-plane shear stress components, obtained in both programmes (Abaqus and CAM) are: $\tau_{ab} = \sigma_{ab} = \sigma_{ba} = -100$ MPa. These match exactly the analytical value. Therefore, it can be concluded, that the modified criteria in this test yield the same damage onset estimation as the

standard ones. Moreover, the differences between the analyzed approaches in the states which are close to the pure in-plane shear will be negligible.

5.2. Compressed plate

Secondly, a compressed plate similarly as in [48] is studied. Geometry of the plate together with loads, surface coordinate system ($t_1 - t_2$) and boundary conditions (BCs) are depicted in Figure 5.

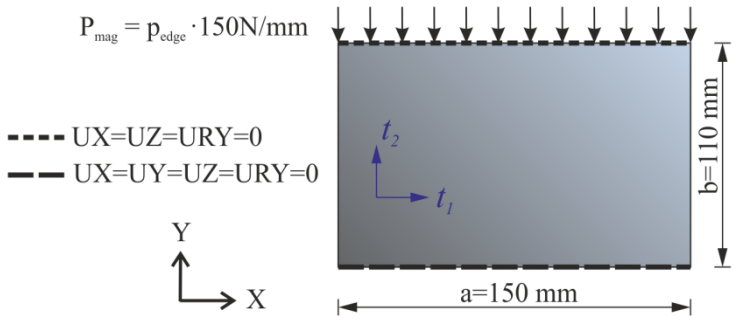

Figure 5. Geometry, surface coordinate system, loads and BCs of the compressed plate

Geometrically non-linear analysis is carried out. Since the plate may lose its stability, a force imperfection is imposed. The imperfection recover a deformation pattern consistent with the 1st buckling mode (the plate buckles into one half-wave along its shorter edge). The FPF load (magnitude of the edge load) is estimated here by means of Hashin criterion. The failure indices are monitored at points that match the in-plane integration rules, specific for each used element, and 3 points regularly distributed in the thickness direction of each layer. S4 shell finite element is used in Abaqus calculations, while CAMe16FI shell element is utilized in CAM. Therefore, the locking effect can be treated as negligible. Mesh of 925 nodes is created in both codes. The material elastic and strength properties of a single lamina are: $E_a = 37.24$ GPa, $E_b = 10.04$ GPa, $G_{ab} = G_{ac} = 4.92$ GPa, $G_{bc} = 2.83$ GPa, $v_{ab} = 0.24$, $X_t = 788.1$ MPa, $X_c = 243.5$ MPa, $Y_t = 43.45$ MPa, $Y_c = 109.9$ MPa, $S_l = 31.32$ MPa,

$S_t = 9.7$ MPa. The single ply thickness is equal to 0.127 mm, whereas the lamination sequence is $[\pm 45]_s$, regarding t_1 direction.

It is observed in both FEA codes that the damage initiation occurs just after buckling of the plate due to the matrix tension mode. The calculated edge load magnitude, corresponding to the FPF load, is equal to 181.4 N in Abaqus (standard Hashin criterion) and 181.8 N in CAM (modified Hashin criterion). FPF location is approximately the same (relative to shell surface integration points position) in two programs and is observed in +45° external ply, in the vicinity of the free edge (see Figure 6). However, different stress states give the rise to the following stress failure, namely: $\sigma_{bb} = 17.14$ MPa, $\tau_{ab} = -28.71$ MPa, $\sigma_{aa} = 44.49$ MPa are observed in Abaqus, while $\sigma_{bb} = 15.45$ MPa, $\sigma_{ba} = -29.26$ MPa, $\sigma_{aa} = 41.57$ MPa, $\sigma_{ab} = -28.47$ MPa are found in CAM. Patterns of matrix tension failure indices, at the moment when FPF load capacity is achieved, in the external +45° ply are shown for Abaqus and CAM in Figure 6.

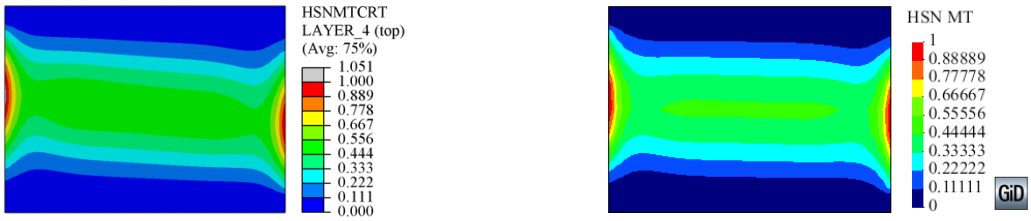

Figure 6. Matrix tension failure indices in +45 external ply, obtained in Abaqus (left) and CAM (right), at the moment of damage initiation

The estimated experimental FPF load is close to the experimental buckling load which is 195±12.3 N [48] and the failure develops from the plate sides [48]. Thus, the present FPF loads correspond well with the reference experimental data. However, they are different than the numerical one in [48], where FPF edge load magnitude is equal to 307.34 N. In view of the present results the solution from [48] seems to be overestimated.

5.3 Cylindrical panel subjected to pressure load

The third example concerns a cylindrical panel subjected to pressure load. A similar one is studied in [49]. Three different panel constant curvatures, defined by *R*/*b* ratio, are analyzed here: $R/b=\infty=$ plate, $R/b=100$ and $R/b=10$. The following material elastic and strength properties of a single ply are used: $E_a=132.4$ GPa, $E_b=10.7$ GPa, $G_{ab}=G_{ac}=5.6$ GPa, $G_{bc}=3.4$ GPa, $v_{ab}=0.24$, $X_t=1514$ MPa, $X_c=1696.7$ MPa, $Y_t=43.8$ MPa, $Y_c=43.8$ MPa, $S_l=87$ MPa. Each ply has thickness 0.127 mm and $[0/90]_s$ stacking sequence is assigned to the panel. The panel geometry, surface coordinate system (t_1-t_2), loads and BCs are shown in Figure 7.

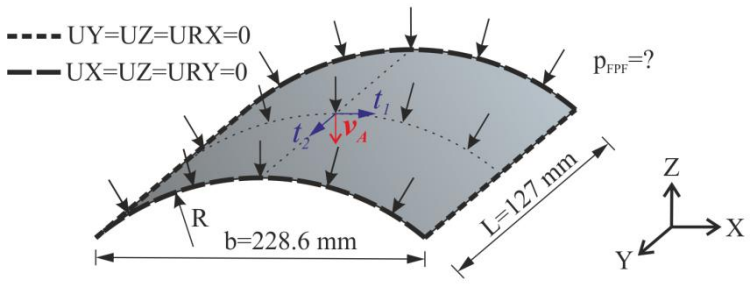

Figure 7. Geometry, surface coordinate system, loads and BCs of the cylindrical panel

The Tsai-Wu criterion is used to predict FPF pressures. Two types of analyses are carried out: linear and non-linear one. Full panel is studied in the linear analysis, in which 8×8 mesh is used similarly as in [49]. The S8R element is used in Abaqus calculations and the CAMe9FI shell element, in which the locking effect is judged on the basis of some additional tests to be negligible is utilised in CAM. The failure indices are checked at element integration points in the middle of each layer.

Moreover, geometrically non-linear solution is presented here as additional calculation. Only quarter of the panel is studied in this case, since the geometry, lamination sequence, BCs and loads are doubly symmetric. New structural meshes are created for

nonlinear calculations, comprising 9017 nodes in Abaqus (S4 elements) and 9271 nodes in CAM (CAMe16FI element described earlier). The failure indices in nonlinear solution are checked in external and middle faces of each layer, which we believe is more appropriate approach in comparison with the one given in [49], where the indices are checked only in the middle of each layer. The FPF pressures following from linear and non-linear calculations are shown in Table 3. The plot of actual pressure versus v_A displacement (see Fig. 5) measured during the non-linear analysis is presented in Figure 8.

Table 3. FPF pressures for the cylindrical panel [kPa]

R/*b*	linear solution			non-linear solution	
	Prusty, Satsanagi, and Ray [49]	Abaqus S8R	CAM e9FI	Abaqus S4	CAM e16FI
10	16.93	16.93	16.55	10.1	9.87
100	4.31	4.47	4.49	11.7	11.41
plate	4.08	4.23	4.21	12.0	11.72

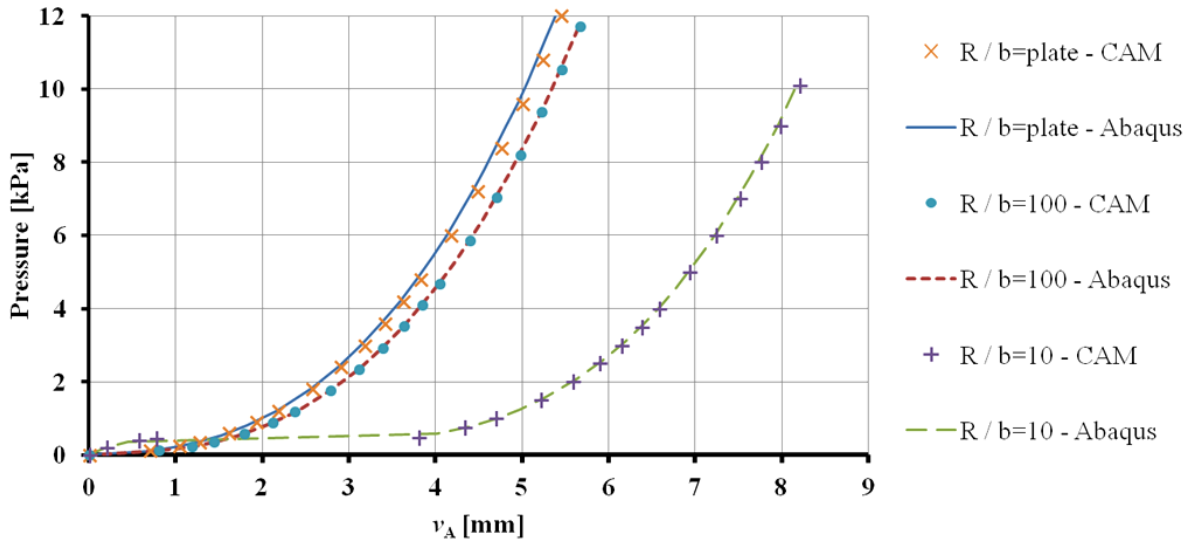

Figure 8. Actual pressure versus v_A displacement.

The linear results presented in Table 1 are in good correspondence with the reference solution [49]. Negligibly small shear components asymmetry is observed during the linear calculations in the vicinity of failed ply located in the centre of the panel for $R/b = \text{plate}$ and $R/b = 100$. Hence, classical Tsai-Wu criterion (Abaqus) and modified one (CAM) results are

very close to each other. For $R/b=10$ there is a small difference between Abaqus and CAM solutions of linear computations. Small asymmetry of the shear stress components is observed in analysis. The failure starts to develop close to the panel corner. The surface integration points of fully integrated element lie closer to the panel corner than the one matching the reduced integration scheme, which possibly cause this difference in FPF predictions. This effect has been discussed e.g. in [50].

According to Figure 8 we may state that the response of the panel is definitely nonlinear and, therefore the FPF non-linear pressure estimations are significantly distinct than the linear ones, as it is compared in Tab. 3. The discrepancy between the non-linear Abaqus and CAM results is small. It may be attributed to the response of the structure, which is a little bit stiffer in Abaqus. A very low shear stress asymmetry is observed in this task that do not affect FPF estimations.

At this stage it can be concluded that for regular, smooth shells we do not observe significant differences between results obtained on the basis of classical and modified criteria. This corresponds with the authors earlier experiences concerning analyses of shell structures made of isotropic, homogenous elastic and plastic materials ([18], [26], [27], [47]). It should be emphasised that in 5-parameter shell theories, implemented in many commercial codes, the sixth degree of freedom, which is necessary in the analysis of irregular shells, is introduced as an artificial rotational stiffness perpendicular to the shell reference surface, see e.g. [51] . The stiffness value is selected on the basis of some numerical experiments. Therefore, it is expected that some differences in the results will emerge during analysis of irregular shells, to which the nonlinear 6p shell theories as the present one or [52] are dedicated.

5.3. Rib-stiffened, partially clamped panel

Consequently, in the following study irregular shells are considered. Firstly, we analyse a rib-stiffened, partially clamped panel, subjected to a concentrated force. This example is motivated by the work [53]. The geometry of the panel, surface coordinate systems ($t_1 - t_2$), BCs and loads are shown in Figure 9.

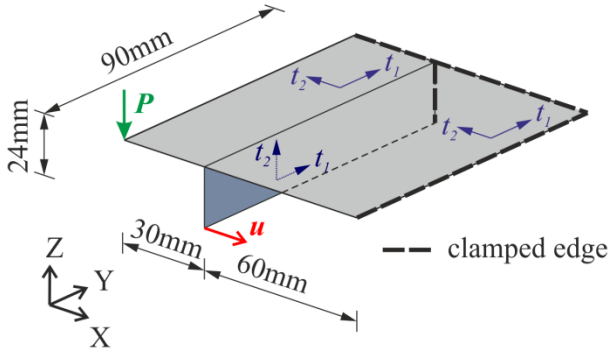

Figure 9. Geometry, loads, surface coordinate systems and BCs of the rib-stiffened panel

The whole panel is made of unidirectional layers combined as $[0/90/\pm45]_s$ sequence relative to the t_1 direction (see Figure 9). The single layer is endowed with the following material and strength properties (as in [53]): $E_a = 130$ GPa, $E_b = 10$ GPa, $G_{ab} = G_{ac} = 4.85$ GPa, $G_{bc} = 3.62$ GPa, $\nu_{ab} = 0.31$, $X_t = 1933$ MPa, $X_c = 1051$ MPa, $Y_t = 51$ MPa, $Y_c = 141$ MPa, $S_l = 61$ MPa, $S_t = 30.5$ MPa. Tsai-Wu and Hashin criteria are used to predict the damage in geometrically non-linear analysis.

We expect differences between FPF loads estimated by the standard (Abaqus) and modified criteria (CAM), which are related only to the used theories. In order to prove it, we carry out some analyzes with aid of CAMe4URI, S4R, CAMe16FI and S4 elements.

Firstly we run preliminary analysis with concentrated force equal to P=30N and various reduced integration finite elements, namely CAMe4URI and S4R, using the same mesh density. CAMe4URI is a 4-node element with uniformly reduced integration (URI, 1×1)

technique and no additional hourglass control. The S4R element has hourglass control included in its formulation. To make S4R similar to CAMe4URI it is necessary to deactivate hourglass control. Hence, we set membrane and bending hourglass stiffness's of S4R elements as small as it is possible, which in this case is $\gamma = 10^{-9}$. For the 4-node finite elements a structural mesh of 2 668 nodes is used, created by the following edge divisions: 15 elements across the narrower part of the plate (to the left of the stiffener), 12 elements across the stiffener, 30 elements across the wider part of the plate (to the right of the stiffener), 45 elements along the panel [(15+12+30)×45 elements].

Since reduced integration elements may exhibit hourglass modes, their results are compared with the ones obtained using CAMe16FI and S4 elements described earlier. The mesh division for 4-node elements can be easily adjusted to CAMe16FI elements without the change of total number of nodes i.e. (5+4+10)×15 16-node elements. The obtained equilibrium paths are compared in Figure 10. As it can be noted the obtained results present very good agreement. However, the same is not true when stress distribution between standard and 6p theories is taken into account.

Figure 11 depicts the changes of in-plane shear stresses (at integration points) in the plate in its top layer for the CAMe4URI, S4R (with hourglass control $\gamma = 10^{-9}$), CAMe16FI and S4 elements in the portrayed cross section. This particular location, denoted by dashed line in Figure 11, contains the position where FPF appears in further calculations.

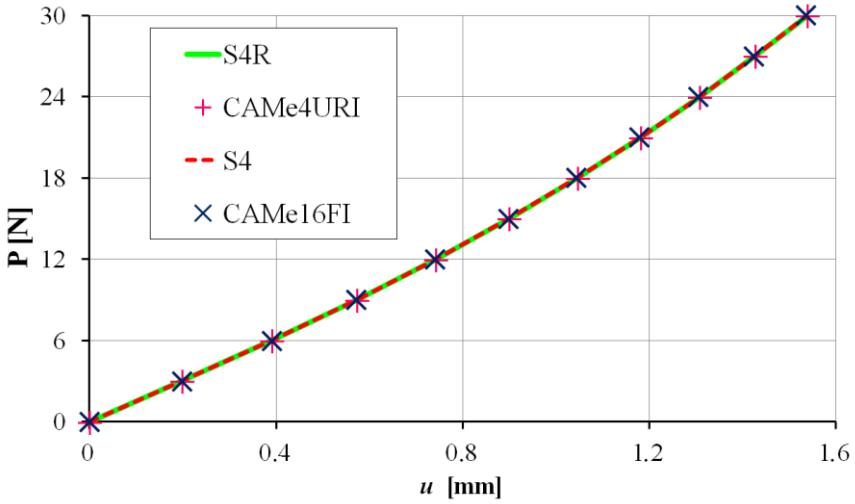

Figure 10. Actual value of force P vs. u displacement in the analysis of rib-stiffened panel

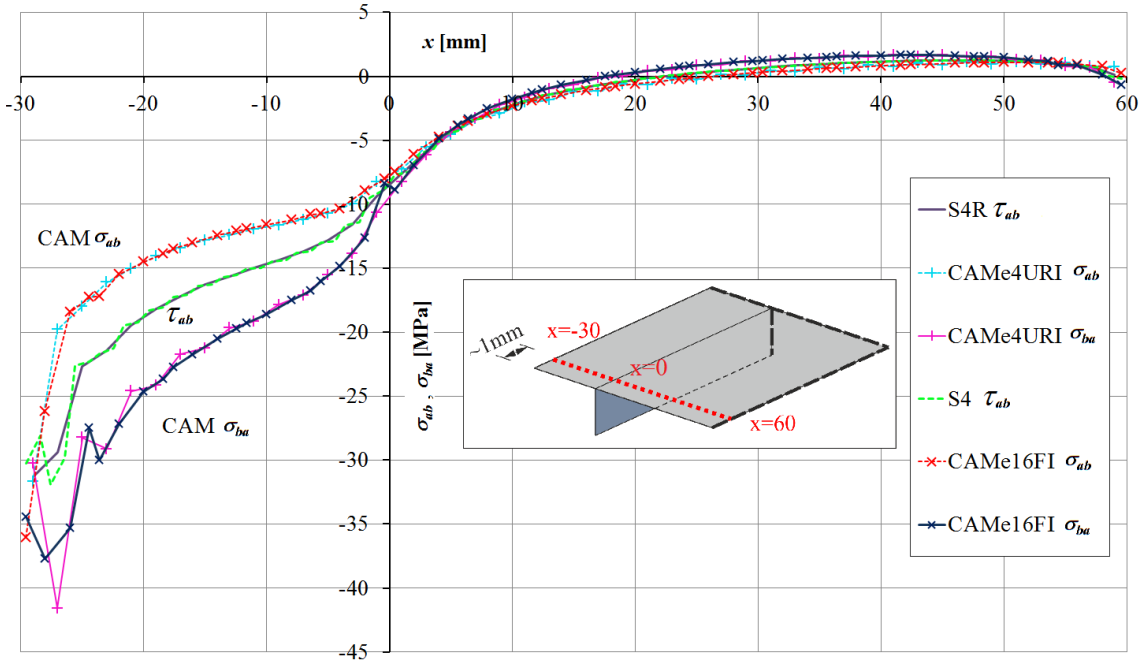

Figure 11. The in-plane shear stresses in the plate, along the shown line, results for CAMe4URI, S4R (with hourglass control $\gamma = 10^{-9}$), CAMe16FI and S4 in top layer

In order to make the interpretation of Figure 11 easier, its part for $x \in [-30, 0]$ is shown in Figure 12 and for $x \in [15, 60]$ in Figure 13.

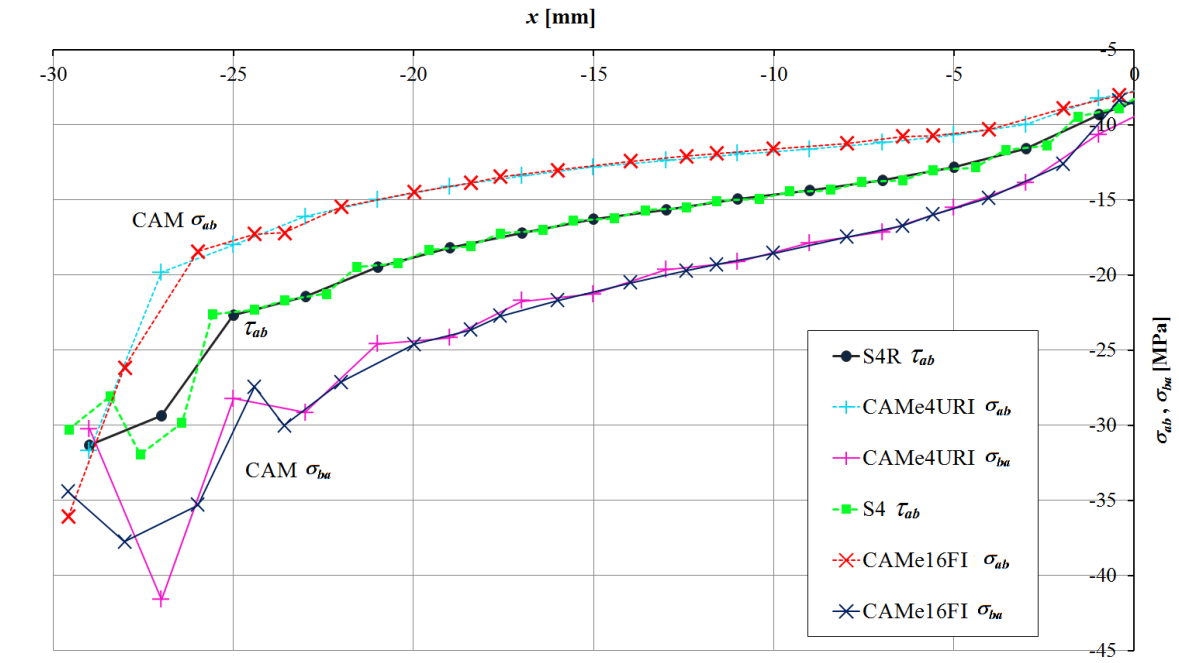

Figure 12. The in-plane shear stresses in the plate, results for CAMe4URI, S4R (with hourglass control, $\gamma = 10^{-9}$), CAMe16FI and S4 in top layer, $x \in [-30, 0]$

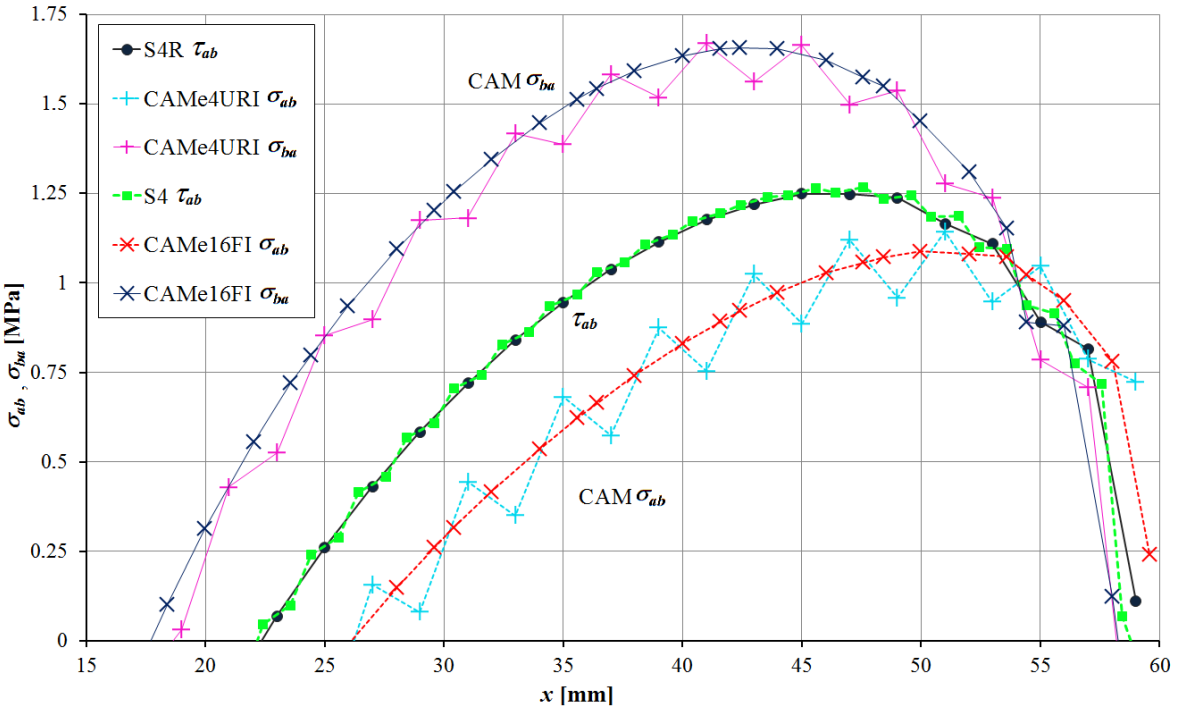

Figure 13. The change of in-plane shear stresses in the plate, results for CAMe4URI, S4R (with hourglass control, $\gamma = 10^{-9}$), CAMe16FI and S4 in top layer, $x \in [15, 60]$

All distinctions in the predicted stress state, regarding Abaqus and CAM, maintain the same character of in-plane shear stress change (see graphs in Figure 11). Therefore, this trend comes from the application of accordingly 5 or 6 parameter theory and is independent from the used finite elements.

It can be stated on the basis of Figure 11, Figure 12, Figure 13 that evident asymmetry of in-plane shear stress appears in CAM results, which is not visible in Abaqus solution. The difference between CAMe4URI and CAMe16FI results follows from different number of integration points and is typical for the applied techniques of URI and FI. Spurious zero-energy effect is noticeable in CAMe4URI result. Thus we use only higher order FI elements in 6p theory.

To compute the value of FPF load we use CAMe16FI elements and S4 as well. The values of failure initiation are monitored at integration points, in 3 locations across each layer (top, middle bottom). The following FPF loads are found during calculations with CAMe16FI: 27.9N for the modified Tsai-Wu criterion and 28.65N for the modified Hashin criterion. The corresponding values obtained with aid of S4 element in Abaqus, by means of standard criteria are: 29N and 29.95N. The initial failure is observed in all cases in the top layer in the plate over the stiffener. The damage initiates because of matrix tension in both codes, when Hashin criterion is utilised. Figure 14 portrays contours of the Hashin matrix tension failure index in the top layer of the panel in the considered codes.

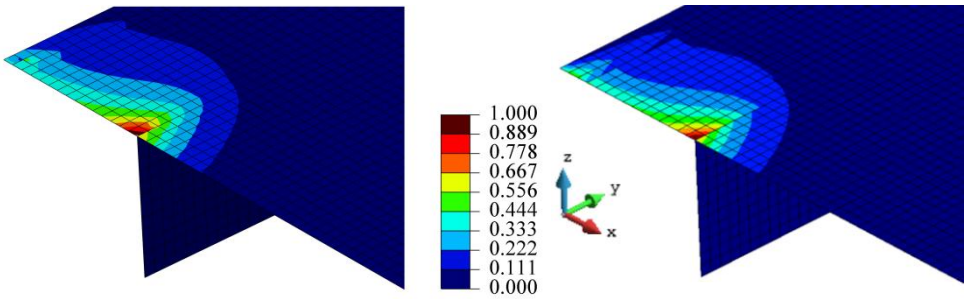

Figure 14. Hashin matrix tension failure index in the top layer of the panel, S4 in Abaqus (left) and CAMe16FI (right).

5.4. Rib-stiffened, partially clamped compressed panel

We analyse rib-stiffened compressed panel. A similar one is studied in [53]. Properties of the panel such as geometry, surface coordinate system ($t_1 - t_2$) loads and boundary conditions are portrayed in Figure 15. $[0/90/\pm45]_s$ ("A" sequence) is the standard lamination scheme applied to the structure. The stacking sequence in the area of stiffener is $[0/90/+45/0/-45]_s$ ("B" sequence), as shown in Figure 15. A single ply is 0.125mm thick. Each lamina has following elastic and strength properties: $E_a = 130$ GPa, $E_b = 10$ GPa, $G_{ab} = G_{ac} = 4.85$ GPa, $G_{bc} = 3.62$ GPa, $v_{ab} = 0.31$, $X_t = 1933$ MPa, $X_c = 1051$ MPa, $Y_t = 51$ MPa, $Y_c = 141$ MPa, $S_l = 61$ MPa, $S_t = 30.5$ MPa.

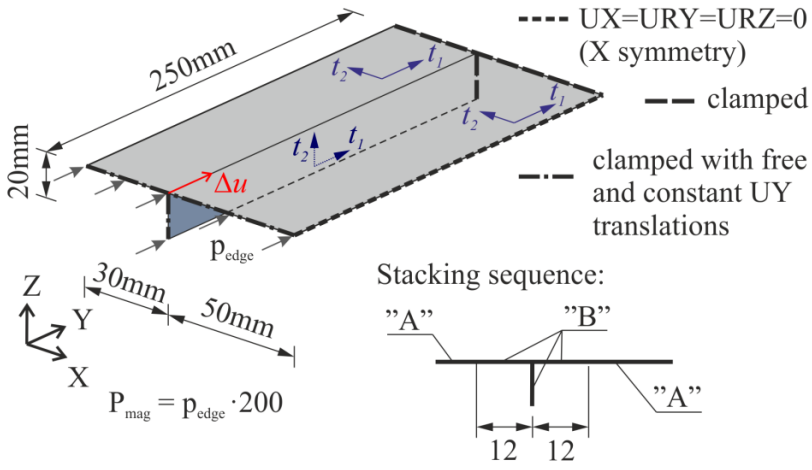

Figure 15. Geometry, surface coordinate systems, loads and BCs of the blade-stiffened compressed panel

According to the experimental data given in [53], the panel loses stability. Hence, load imperfection is introduced. Tsai-Wu and Hashin criteria are used for the purpose of damage onset prediction. The values of failure initiation indices are monitored at integration points in external and middle fibres of each layer. Two variants of finite element mesh are proposed in CAM, both based on the same concept, namely: 3 elements (shorter part) + 4 elements (longer part) are applied across the panel plate together with 2 elements in direction of the rib stiffener cross section, consequently 20 elements are used along the panel. CAMe9FI is utilised in the first mesh variant (total number of nodes equal to 779), while CAMe16FI in the second one (total number of nodes equal to 1708). Such an approach allows for "*p*" type mesh convergence check. It is found out in the course of analysis that aforementioned meshes lead to almost the same global structural behaviour (see Figure 16). Mesh comprising CAMe16FI elements is considered in further FPF analyses, as it provides more detailed information about the panel response. The computational cost is still low in this case. Only one mesh variant is created in Abaqus. It corresponds to the finally chosen CAM one. It has the same total

number of nodes, however S4 elements are created. Load - displacement (P_{mag} - Δu) relation for this task for different considered meshes are shown in Figure 16.

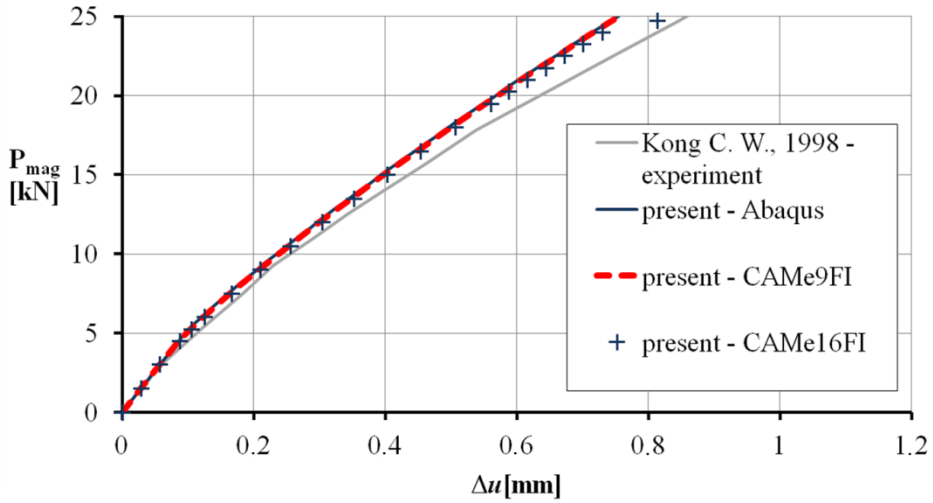

Figure 16. Equilibrium load-displacement (P_{mag} - Δu) paths

The calculated FEM panel response is similar to the experimental one. The FPF is observed for the state of deformation with two buckling half-waves along its length. This corresponds with [53]. As it was previously mentioned, FPF loads are checked only for Abaqus and CAM fine meshes. The following P_{mag} loads are obtained for Tsai-Wu criterion: Abaqus - 21.3kN (classical criterion), CAM - 20.6kN (modified criterion). Regarding Hashin criterion, the P_{mag} load corresponding to the FPF load capacity observed in Abaqus equals approximately 24.3kN (classical criterion), whereas in CAM it is close to 23.6kN (modified criterion). A quantitative difference between Abaqus and CAM results is observed in this example. The failure in both cases occurs due to the matrix tension mode at the plate-blade stiffener connection (see Figure 17). Contours of Hashin criterion matrix tension failure indices at the moment of failure initiation in Abaqus and CAM are shown in Figure 17.

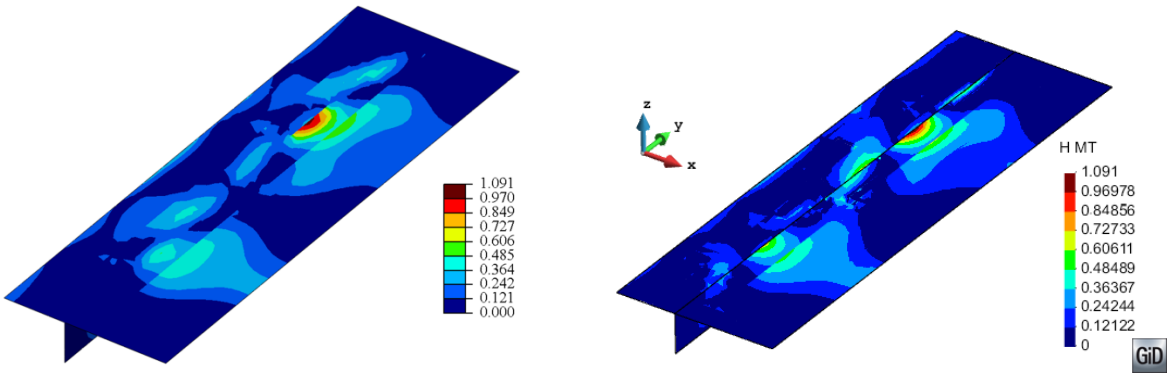

Figure 17. Matrix tension failure indices, maximum value envelope from all layers obtained in Abaqus (left) and CAM (right) at the moment of damage initiation

According to the experimental data given in [53], FPF occurs because of matrix cracking at the load level of 23.82kN. Thus, it can be concluded that the loads obtained with Tsai-Wu criteria versions do not precisely match this value. It seems that the Tsai-Wu criterion is not the most appropriate choice for this geometry and boundary conditions of the problem. The FPF Hashin results are in good correspondence with the experimental data [53]. The FPF loads observed in CAM are slightly lower than the Abaqus ones for both considered failure initiation criteria. Moreover, the FPF estimation according to the Hashin modified criterion obtained in CAM is closer to the experimental [53] value, as compared with the Abaqus one. What is more, some additional in-plane shear stress asymmetry arises in CAM, which also affects the FPF load predictions.

5.5. C-shaped compressed column

Finally, the C-shaped compressed column is analyzed following [54]. It represents an irregular shell structure. It is worthy of noticing that the C-shape column (or beam) is popular benchmark problem for shell elements with drilling rotation see for instance [17][52][55][56].

The geometry of the column analyzed here, together with surface coordinate systems ($t_1 - t_2$), loads and BCs, is depicted in Figure 18.

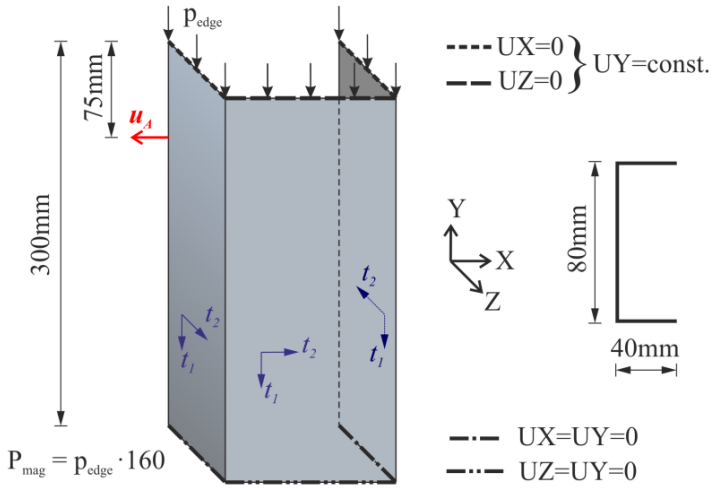

Figure 18. Geometry, surface coordinate systems, loads and BCs of the compressed column

Since it is predicted that the column will lose its stability, a force imperfection is applied. A stacking sequence of $[0/\pm45/90]_s$ is assigned to the column, relative to the t_1 directions, shown in Figure 18. Each ply is 0.131 mm thick and has the following elastic and strength properties: $E_a = 130.71$ GPa , $E_b = 6.36$ GPa , $G_{ab} = G_{ac} = 4.18$ GPa , $G_{bc} = 1.0$ GPa , $v_{ab} = 0.24$, $X_t = 1867.2$ MPa , $X_c = 1531$ MPa , $Y_t = 25.97$ MPa , $Y_c = 214$ MPa , $S_l = 100.15$ MPa . Structural mesh of S4 finite elements, created in Abaqus, contains 4557 nodes. The similar one is built in CAM. It comprises of CAMe16FI elements with total number of 4459 nodes. Geometrically nonlinear calculations are performed, in which Tsai-Wu criterion is used in order to predict the onset of damage. The values of failure initiation criterion indices are monitored at integration points in external and middle fibres of each layer Equilibrium load-displacement paths (P_{mag} - u_A) obtained during the analysis are shown in Figure 19.

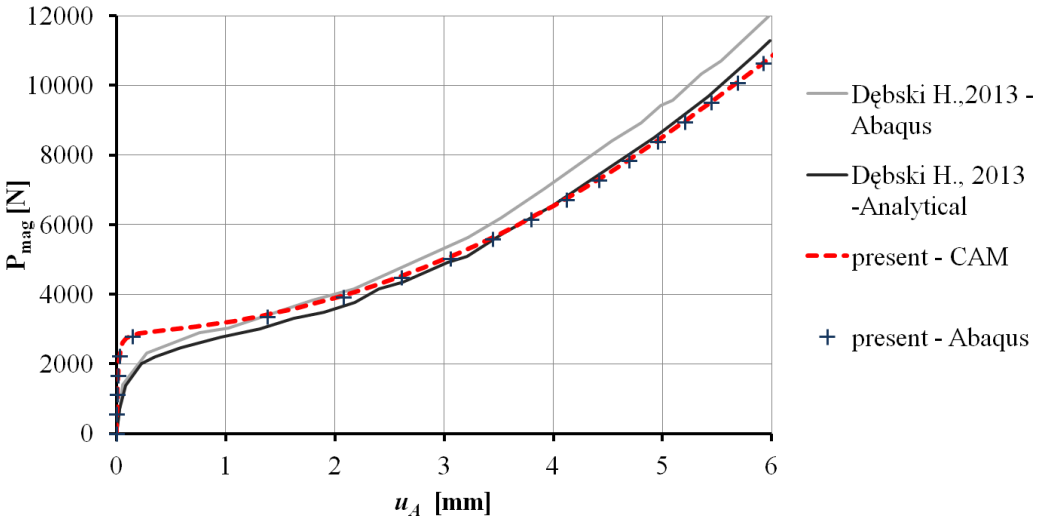

Figure 19. Equilibrium load-displacement paths (P_{mag} - u_A)

The response of the structure obtained in present calculations is similar to the one presented in [54] in the post-buckling range. Global behaviour of the structure obtained in present Abaqus and CAM calculations is nearly the same. The P_{mag} load reported in [54], which causes FPF according to the classical Tsai-Wu criterion, yields 10122.5 N. The corresponding failure loads obtained in the Authors calculations are approximately 9965 N - Abaqus (classical Tsai-Wu failure criterion) and 9830 N - CAM (modified Tsai-Wu failure criterion), and are comparable with the one given in [54]. The FPF occurs in the present calculations in the bottom layer of the lowest ply (0 direction). Contours of the Tsai-Wu failure index for the aforementioned lamina are shown in Figure 20 for both codes.

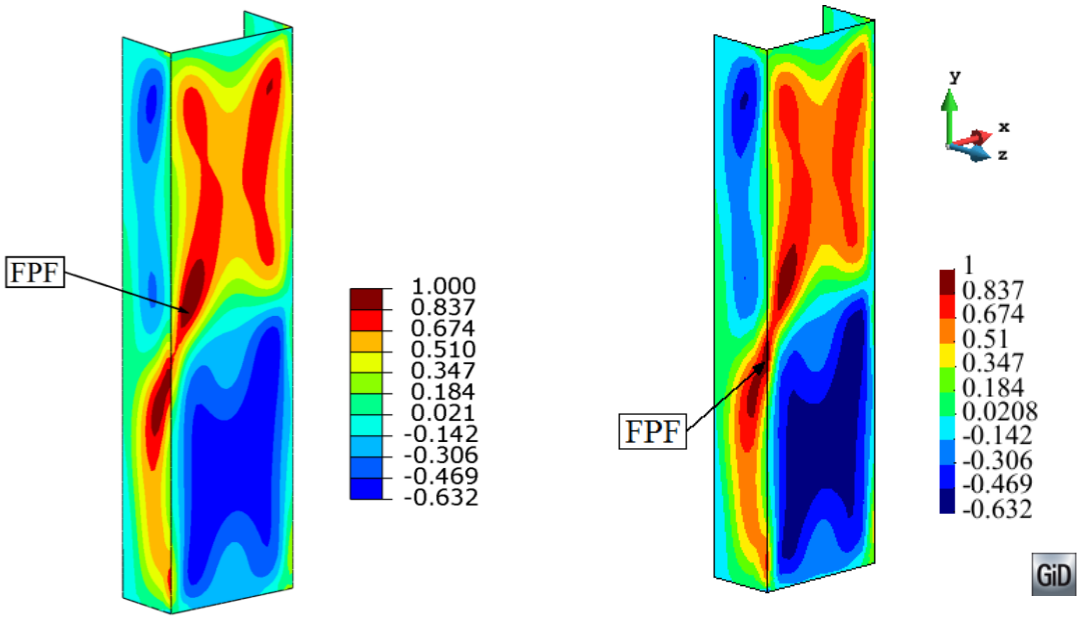

Figure 20. Tsai-Wu failure index contours in the bottom layer of the lowest ply (0 direction); the left side - classical criterion (Abaqus), the right side - modified criterion (CAM)

Despite the fact that the global compressive force, which causes FPF, yields similar values in present calculations, different failure locations within the same aforementioned ply are observed in Abaqus and CAM. In Abaqus the failure initiates within the column web slightly above the structure mid length, while in CAM the damage occurs on the column flange in the vicinity of flange-web connection, a little bit below the column mid length. This difference is attributed to the drilling rotation effect, which can be caught only in the non-linear 6p shell theory. It is observed in the area of complex deformations, where the buckling half-waves change their sides. What is more interesting, the difference constitutes a qualitative change in obtained results, in which the failure location area is moved to the edge of the shell irregularity. As a consequence, moderate shear components asymmetry appears in CAM result. The stress state, which produce the failure in CAM is $\sigma_{aa} = -201.1$ MPa $\sigma_{bb} = 21.91$ MPa, $\sigma_{ba} = 31.33$ MPa ($\sigma_{ab} = 22.39$ MPa). This is also the reason why the P_{mag} load obtained in CAM is slightly lower in comparison with the one from Abaqus.

6. Conclusions

A brief description of non-linear 6p shell theory and a particular constitutive relation for laminated composites is given in this work. Modifications of Tsai-Wu and Hashin failure criteria are proposed, which follow the assumptions of the aforementioned approach. To verify if these modifications allow to estimate FPF load capacities properly some FEA are carried out. The analyzes of compressed plate and cylindrical panel subjected to pressure revealed that it is possible to analyze laminated shell structures, regarding the description of their initial failure, by means of the non-linear 6p shell theory. The FPF loads for modified criteria yield similar results as for classical ones, when there is no big difference between σ_{ab} and σ_{ba} in-plane shear stress components. The authors results correspond also well with the reference values for similar analyses. Some essential conclusions follow from the analyzes of the rib-stiffened, partially clamped panel, rib-stiffened, partially clamped compressed panel and the compressed column with C-cross section. It is observed that additional effects connected with drilling rotation may develop, even if the global force-displacement response is similar as for standard theory with symmetric strain and stress measures. The drilling rotation in the non-linear 6p shell theory is not introduced artificially. Therefore, behaviour of irregular, multifold shells can be predicted in a more detailed way. Additionally, as a consequence of the constitutive relation some in-plane shear stress components asymmetry arises, that also affects FPF estimations. We believe that the 6p shell theory allow one to predict more detailed deformations of shells. This together with the proposed criteria modifications results in different FPF estimations, as compared with 5p theory.

Appendix

To establish explicit form of matrices from (21)-(24) we further assume that the shell under discussion is sufficiently thin so that $\mu \approx 1$. As thin shell we define the shell which thickness

h is substantially smaller than typical dimension L and the curvature radius $R_{\min}$ is smaller than h. Hence

$$\underset{4\times4}{\mathbf{A}} = \sum_{k=1}^{N_L} \{\boldsymbol{C}_m\}_k \left(\zeta_k^+ - \zeta_k^-\right), \qquad \underset{4\times4}{\mathbf{B}} = \tfrac{1}{2} \sum_{k=1}^{N_L} \{\boldsymbol{C}_m\}_k \left((\zeta_k^+)^2 - (\zeta_k^-)^2\right), \tag{A.1}$$

$$\underset{4\times4}{\mathbf{D}} = \tfrac{1}{3} \sum_{k=1}^{N_L} \{\boldsymbol{C}_m\}_k \left((\zeta_k^+)^3 - (\zeta_k^-)^3\right), \qquad \underset{2\times2}{\mathbf{S}} = \sum_{k=1}^{N_L} (\alpha_s)_k \{\boldsymbol{C}_s\}_k \left(\zeta_k^+ - \zeta_k^-\right). \tag{A.2}$$

In the case of the drilling couples we proposed in [33] to use the relation

$$\mathbf{s}_d = \alpha_t \sum_{k=1}^{N_L} \left(\int_{\zeta_k^-}^{\zeta_k^+} (\alpha_t)_k \{\boldsymbol{C}_d\}_k \boldsymbol{\varepsilon}_d \, \mu \, d\zeta \right) = \underset{2\times2}{\mathbf{G}} \boldsymbol{\varepsilon}_d . \tag{A.3}$$

Here constitutive matrices $\boldsymbol{C}_m$ and $\boldsymbol{C}_s$ are defined from (20) through orthogonal transformations

$$\boldsymbol{C}_m = \tilde{\mathbf{T}}_m^{-1} \tilde{\boldsymbol{C}}_m \tilde{\mathbf{T}}_m , \qquad \boldsymbol{C}_s = \tilde{\mathbf{T}}_s^{-1} \tilde{\boldsymbol{C}}_s \tilde{\mathbf{T}}_s , \tag{A.4}$$

$$\tilde{\mathbf{T}}_k = \left[\begin{array}{cccc|cc} C^2 & S^2 & SC & SC & 0 & 0 \\ S^2 & C^2 & -SC & -SC & 0 & 0 \\ -SC & SC & C^2 & -S^2 & 0 & 0 \\ -SC & SC & -S^2 & C^2 & 0 & 0 \\ \hline 0 & 0 & 0 & 0 & C & -S \\ 0 & 0 & 0 & 0 & S & C \end{array}\right]_k = \left[\begin{array}{c|c} \tilde{\mathbf{T}}_m & \mathbf{0}_{4\times2} \\ \hline \mathbf{0}_{2\times4} & \tilde{\mathbf{T}}_s \end{array}\right]_k , \tag{A.5}$$

and in (A.3) is assumed as $\boldsymbol{C}_d = \zeta^2 \boldsymbol{C}_s$.

ACKNOWLEDGEMENT

This support is gratefully acknowledged. B. Sobczyk is supported under Gdansk University of Technology (Poland), Faculty of Civil and Environmental Engineering, Young Scientist Support Program. Abaqus calculations were carried out at the Academic Computer Centre in Gdańsk, Poland.

Bibliography

[1] F. C. Campbell, Structural Composite Materials, ASM International, Materials Park Ohio, 2010.

[2] Ł. Mazurkiewicz, J. Małachowski, and P. Baranowski, Optimization of protective panel for critical supporting elements. Compos. Struct., vol. 134, pp. 493-505, 2015.

[3] E. Reissner, Linear and nonlinear theory of shells, in Y.C. Fung, and E.E. Sechler (eds.), Thin Shell Structures, pp. 29–44, Prentice-Hall, Englewood Cliffs, 1974.

[4] A. Libai, and J.G. Simmonds, The Nonlinear Theory of Elastic Shells, 2nd edn, Cambridge University Press, Cambridge, 1998.

[5] W. Pietraszkiewicz , Refined resultant thermomechanics of shells, Int. J. Eng. Sci., vol. 49, pp. 1112-1124, 2011.

[6] W. Pietraszkiewicz, and V. Konopińska, Drilling couples and refined constitutive equations in the resultant geometrically non-linear theory of elastic shells, Int. J. Solids Struct., vol. 51, pp. 2133-2143, 2014.

[7] V. A. Eremeyev, and L. P. Lebedev, Existence theorems in the linear theory of micropolar shells, Z. Angew. Math. Mech, vol. 91, pp. 468-476, 2011.

[8] V. A. Eremeyev, L.P. Lebedev, and M. J. Cloud, The Rayleigh and Courant variational principles in the six-parameter shell theory, Math. Mech. Solids, vol. 20, pp. 806-822, 2014.

[9] M. Bîrsan, and P. Neff, Existence of minimizers in the geometrically non-linear 6-parameter resultant shell theory with drilling rotations, Math. Mech. Solids, vol. 19, pp. 376-397, 2014.

[10] M. Bîrsan, and P. Neff, Existence theorems in the geometrically non-linear 6-parameter theory of elastic plates, J. Elasticity, vol. 112, pp. 185–198, 2013.

[11] V. A. Eremeyev, and W. Pietraszkiewicz, Material symmetry group and constitutive equations of micropolar anisotropic elastic solids, Math. Mech. Solids., (published online before print on May 7, 2015)

[12] V.A. Eremeyev, and W. Pietraszkiewicz, Thermomechanics of shells undergoing phase transition, J.Mech. Phys. Solids, vol. 59, pp. 1395-1412, 2011

[13] H. Altenbach, and V. A. Eremeyev, Vibration Analysis of Non-linear 6-parameter Prestressed Shells, Meccanica, vol. 49, pp. 1751-1761, 2014.

[14] W. Pietraszkiewicz , and V.Konopińska, Junctions in shell structures: A review, Thin Wall. Struct., vol. 95, pp. 310–334, 2015.

[15] J. Chróścielewski, J. Makowski, and H. Stumpf, Genuinely resultant shell finite elements accounting for geometric and material non-linearity, Int. J. Numer. Meth. Eng., vol. 35, pp. 63–94, 1992.

[16] J. Chróścielewski, J. Makowski, and W. Pietraszkiewicz, Statics and Dynamics of Multifold Shells: Nonlinear Theory and Finite Element Method (in Polish), IPPT PAN, Warsaw, 2004.

[17] J. Chróścielewski, and W. Witkowski, 4-node semi-EAS element in 6–field nonlinear theory of shells, Int. J. Numer. Meth. Eng., vol. 68, pp. 1137–1179, 2006.

[18] W. Witkowski, 4-Node combined shell element with semi-EAS-ANS strain interpolations in 6-parameter shell theories with drilling degrees of freedom, Comput. Mech., vol. 43, pp. 307–319, 2009.

[19] J. Chróścielewski, W. Pietraszkiewicz, and W. Witkowski, On shear correction factors in the non-linear theory of elastic shells, Int. J. Solids Struct., vol. 47, pp. 3537–3545, 2010.

[20] J. Chróścielewski and W. Witkowski Discrepancies of energy values in dynamics of three intersecting plates, Int. J. Numer. Meth. Biomed. Engng. 2010; 26:1188–1202

[21] Makowski J., and Stumpf H., Mechanics of Irregular Shell Structures, Mitteilung Nr. 95, Institut für Mechanik, Bochum: Ruhr-Universität, 1994.

[22] H. Altenbach, and V.A. Eremeyev, On the linear theory of micropolar plates, Z. Angew. Math. Mech., vol. 89, pp. 242–256, 2009.

[23] J. Chróścielewski, and W. Witkowski, On some constitutive equations for micropolar plates, Z. Angew. Math. Mech., vol. 90, pp. 53–64, 2010.

[24] J. Chróścielewski, and W. Witkowski, FEM analysis of Cosserat plates and shells based on some constitutive relations, Z. Angew. Math. Mech., vol. 91, pp. 400–412, 2011.

[25] W. Nowacki, Couple-stresses in the theory of thermoelasticity, in H. Parkus, and L.I. Sedov (eds.), Irreversible aspects of continuum mechanics and transfer of physical characteristics in moving fluids. IUTAM Symposia Vienna 1966, pp. 259–278, Springer-Verlag, Wien, 1968

[26] S. Burzyński, J. Chróścielewski, and W. Witkowski, Elastoplastic material law in 6-parameter nonlinear shell theory, in W. Pietraszkiewicz, and J. Górski (eds.), Shell Structures: Theory and Applications, vol. 3, pp. 377–380, CRC Press, London, 2014.

[27] S. Burzyński, J. Chróścielewski, and W. Witkowski, Elastoplastic law of Cosserat type in shell theory with drilling rotation, Math. Mech. Solids, vol. 20, pp. 790-805, 2014.

[28] S. Burzyński, J. Chróścielewski, and W. Witkowski, Geometrically nonlinear FEM analysis of 6-parameter resultant shell theory based on 2-D Cosserat constitutive model, Z. Angew. Math. Mech., vol. 1, 2015.

[29] J. Jeong, H. Ramezani, I. Münch, P. Neff, A numerical study for linear isotropic Cosserat elasticity with conformally invariant curvature, Z. Angew. Math. Mech., vol. 89, pp. 552 – 569, 2009.

[30] P. Neff. A geometrically exact Cosserat shell-model including size effects, avoiding degeneracy in the thin shell limit. I. Formal dimensional reduction for elastic plates and existence of minimizers for positive Cosserat couple modulus, Contin. Mech. Thermodyn., vol. 16, pp. 577–628, 2004.

[31] P. Neff, A geometrically exact planar Cosserat shell-model with microstructure: existence of minimizers for zero Cosserat couple modulus, Math. Mod. Meth. Appl. S., vol. 17, pp. 363–392, 2007.

[32] K. Daszkiewicz, J. Chróścielewski, and W. Witkowski, Geometrically nonlinear analysis of functionally graded shells based on 2-d Cosserat constitutive model, Engng. Trans., vol. 62, pp. 109–130, 2014.

[33] J. Chróścielewski, I. Kreja, A. Sabik, and W. Witkowski, Modeling of composite shells in 6-parameter nonlinear theory with drilling degree of freedom, Mech. Adv. Mater. Struct., vol. 18, pp. 403–419, 2011.

[34] V. Ivannikov, C. Tiago, P. M. Pimenta, Meshless implementation of the geometrically exact Kirchhoff–Love shell theory, Int. J. Numer. Meth. Engng 2014; 100:1–39

[35] R. M. Jones, Mechanics of Composite Materials, Taylor & Francis, Philadelphia, 1999.

[36] S. W. Tsai, and E. M. Wu, A General Theory of Strength for Anisotropic Materials, J. Compos. Mater., vol. 5, pp. 58-80, 1971.

[37] Z. Hashin, Failure criteria for unidirectional fiber composites, J. Appl. Mech., vol. 47, pp. 329-334, 1980.

[38] A. Puck, and H. Schürmann, Failure analysis of FRP laminates by means of physically based phenomenological models, Compos. Sci. Technol., vol. 62, pp. 1633-1662, 2002.

[39] J. Chróścielewski, The family of C^0 finite elements in 6-parameter nonlinear shell theory (in Polish), Gdańsk University of Technology research bulletin (in polish), vol. LIII, pp. 1-291, 1996.

[40] J. Chróścielewski, J. Makowski, H. Stumpf, Finite element analysis of smooth, folded and multi-shell structures, Comput. Method. Appl. M., vol. 141, pp. 1-46, 1997.

[41] D. Braess, Finite elements. Theory, fast solvers and applications in solid mechanics, Cambridge University Press, Cambridge, 2007.

[42] M. J. Hinton, A. S. Kaddour, and P. D. Soden (eds.), Failure Criteria in Fibre Reinforced Polymer Composites: The World-Wide Failure Exercise, Elsevier, Amsterdam, 2004.

[43] W. Pietraszkiewicz, and V.A., Eremeyev, On vectorially parameterized natural strain measures of the non-linear Cosserat continuum, Int. J. Solids Struct., vol. 46, pp. 2477-2480, 2009.

[44] A. Ibrahimbegović, On the choice of finite rotation parameters, Comp. Meth. Appl. Mech. Engng., vol. 149, pp. 49-71, 1997.

[45] C. G. Koay, On the six-dimensional orthogonal tensor representation of the rotation in three dimensions: a simplified approach, Mech. Mater., vol. 41, pp. 951–953, 2009.

[46] B. Sobczyk, Laminated plates and shells – first ply failure analysis within 6-parameter shell theory, Proc. YIC GACM 2015 & 3rd ECCOMAS YIC Conf., Aachen, Germany, pp. 1-4, RWTH Aachen, Aachen, 2015.

[47] J. Chróścielewski, W. Witkowski, B. Sobczyk, and A. Sabik. First ply failure analysis of laminated shells undergoing large displacements – 6 parameter shell theory approach. Proc. 3rd PCM & 21st CMM, Gdańsk, Poland, vol. 1, pp. 323-324, Polish Society of Theoretical and Applied Mechanics, Gdańsk, 2015.

[48] M. Heidari-Rarani, S. S. Khalkhali-Sharifi, and M. M. Shokrieh, Effect of ply stacking sequence on buckling behaviour of E-glass/epoxy laminated composites. Comp. Mater. Sci., vol. 89, pp. 89-96, 2014.

[49] B. G. Prusty, S. K. Satsanagi, and C. Ray, First Ply Failure Analysis of Laminated Panels Under Transverse Loading, J. Reinf. Plast. Comp., vol. 20, pp. 671-684, 2001.

[50] A. Sabik, and I. Kreja, Large thermo-elastic displacement and stability FEM analysis of multilayered plates and shells. Thin Wall Struct., vol. 71, pp. 119-133, 2014

[51] O. C. Zienkiewicz, and R. L. Taylor, Finite Element Method (Vol 2), 5th ed., Butterworth-Heinemann, Oxford, 2000.

[52] K. Wiśniewski, Finite rotation shells: Basic equations and finite elements for Reissner kinematics, Springer, Berlin, 2010.

[53] C. W. Kong, I. C. Lee, C. G. Kim, and C. S. Hong, Postbuckling and failure of stiffened composite panels under axial compression. Compos. Struct., vol. 42, pp. 13-21, 1998.

[54] H. Dębski, Numerical Analysis of Stability of Thin-Walled Composite Column with Open Cross-Section. Mechanics and Mechanical Engineering, Vol. 17, pp. 29–35, 2013.

[55] P. Areias, T. Rabczuk, J.M. César de Sá, J.E. Garção, Finite strain quadrilateral shell using least-squares fit of relative Lagrangian in-plane strains, Finite Elements in Analysis and Design 98, 26–40, 2015.

[56] P. Areias, T. Rabczuk , J. César de Sá, ·R. Natal Jorge, A semi-implicit finite strain shell algorithm using in-plane strains based on least-squares, Comput Mech, 55, 673–696, 2015.